Rapid Assays to Test for Flavohemoglobin Inhibitors

A thesis submitted to the Committee of Graduate Studies in partial fulfillment of the requirements for the degree of Master of Science in the Faculty of Arts and Science

Trent University
Peterborough, Ontario, Canada

ABSTRACT

Rapid Assays to Test for Flavohemoglobin Inhibitors

Elías Henao

Giardia intestinalis is a parasitic protozoan that possesses a flavohemoglobin (gFlHb), an enzyme that plays a role in the detoxification of reactive nitrogen species (RNS) and reactive oxygen species (ROS) via its nitric oxide dioxygenase (NOD) activity as well as its NADH-oxidase activity. This enzyme is a potential target for imidazole-based antigiardial drugs that act as ligands of the iron within its heme cofactor. In this work, two rapid and relatively inexpensive assays, the colorimetric Griess assay and a fluorescence assay, were adapted, optimized, and implemented to screen for flavohemoglobin inhibitors in parallel studies that compared the response of gFlHb to that of Hmp (*Escherichia coli* flavohemoglobin) when a group of six different imidazole-based compounds was tested. These assays displayed isotype selectivity, showing how the different drugs elicited different responses from the two enzymes. Comparative results for gFlHb and Hmp revealed that bulkier compounds elicited higher inhibition of Hmp, while smaller compounds resulted in better inhibition of gFlHb, which might be explained by the presence of different amino acid residues in the active sites of the enzymes, with two large amino acid sequence inserts being a unique feature of gFlHb, thus blocking the active site from being reached and blocked by larger compounds.

Keywords: *Giardia intestinalis,* flavohemoglobin, gFlHb, Hmp, Griess assay, DAN, fluorescence spectroscopy, UV-Visible spectroscopy, nitric oxide detoxification, imidazole-based drugs

ACKNOWLEDGEMENTS

TABLE OF CONTENTS

LIST OF TABLES

LIST OF ABBREVIATIONS AND SYMBOLS

DAN	2,3-diaminonaphthalene
DMSO	Dimethyl sulfoxide
FAD	Flavin Adenine Dinucleotide
FHP	*Alcaligenes eutrophus* Flavohemoglobin
FlHb	Flavohemoglobin
FNR	Ferredoxin Nucleotide Reductase
gFlHb	*Giardia intestinalis* Flavohemoglobin
Hmp	*Escherichia coli* Flavohemoglobin
K_i	Inhibition Constant
LDH	Lactate Dehydrogenase
NADH	Nicotinamide Adenine Dinucleotide
NAD(P)H	Nicotinamide Adenine Dinucleotide Phosphate
NAT	Naphthalenetriazole
NED	*N*-(1-naphthyl)ethylenediamine
NO	Nitric Oxide
NOD	Nitric Oxide Dioxygenase
NOS	Nitric Oxide Synthase
PMSF	Phenylmethylsulfonyl Fluoride
RNS	Reactive Nitrogen Species
ROS	Reactive Oxygen Species
rpm	Revolutions per Minute
SDS-PAGE	Sodium Dodecyl Sulfate-Polyacrylamide Gel Electrophoresis
SOD	Superoxide Dismutase
SOR	Superoxide Reductase
TCEP	Tris(2-carboxyethyl)phosphine

1. INTRODUCTION

1.1 Giardiasis

Giardiasis is the most common protozoal infection in humans and is a major cause of waterborne and foodborne diarrhea, traveler's diarrhea, as well as day-care center outbreaks as reviewed by Leung et al. (2019). In 2004, giardiasis was included in the World Health Organization (WHO) neglected diseases initiative (Savioli et al., 2006). Giardiasis is caused by the parasite *Giardia intestinalis* and is transmitted through the fecal-oral route mainly through the ingestion of contaminated food and water (Ortega & Adam, 1997) (Figure 1).

Giardia infections are normally self-limiting and are characterized by a broad range of symptoms that may include diarrhea, cramps, bloating, nausea, and vomiting (Cama & Mathison, 2015). The incubation period tends to be 1 to 2 weeks followed by the onset of the infection, which consists of a feeling of intestinal uneasiness as well as nausea and anorexia (Marshall et al., 1997). Some other symptoms that are often associated with early-onset giardiasis are low-grade fever and chills and, as the infection progresses, symptoms may include explosive, watery, foul-smelling diarrhea, marked abdominal gurgling, distension, belching with a foul taste, as well as upper or mid-gastric cramps. Giardia infections can be acute, asymptomatic, or chronic, leading to severe malabsorption and malnourishment, especially in children (Farthing, 1993). The acute stage typically lasts 3 or 4 days and is hard to recognize as giardiasis given its similarities to traveler's diarrhea caused by other factors (Marshall et al., 1997). As a result of asymptomatic cases, the true number of giardia infections is underreported as hosts do not seek treatment, allowing them to be able to spread the parasite to other individuals.

As of 2002, the estimated number of human infections per year was 280,000,000, being especially prevalent in children in developing countries (Lane & Lloyd, 2002). In many

countries, giardiasis is also the most commonly reported intestinal infection in many

domesticated and wild animals. Giardia is a major cause of waterborne infection outbreaks, with

animal-to-human transmission being a major concern (Olson et al., 2000). Rates of detection for

giardia are variable, being as low as 2-5% in developed or industrialized nations and 20-30% in

developing countries (Farthing, 1993). An analysis of water samples in the United States

detected giardia cysts in 81% of raw freshwater samples and in 17% of filtered water samples.

These are shocking statistics as giardiasis outbreaks are often associated with ingestion of

unfiltered or inadequately chlorinated surface water or groundwater influenced by surface water

(Marshall et al., 1997).
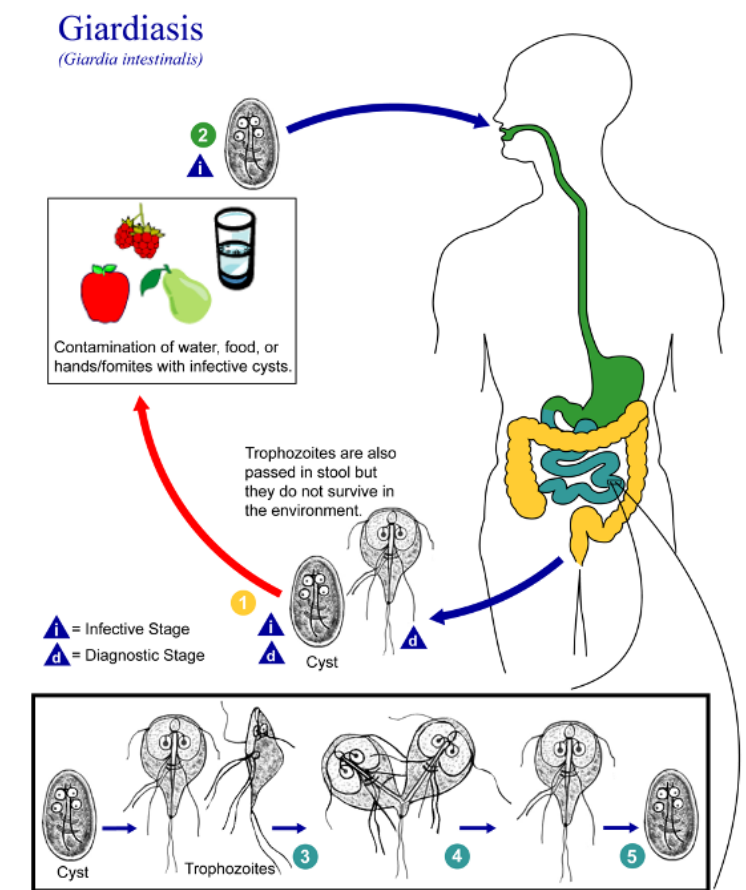
Figure 1: *Giardia life cycle and transmission. Image source: Public Health Image Library, The Centers for Disease Control and Prevention (https://phil.cdc.gov/Details.aspx?pid=3394). This image is in the public domain and is free of copyright restrictions.*

1.2 Giardia

1.2.1 Taxonomy

     Giardia intestinalis, also known as *Giardia duodenalis* or *Giardia lamblia*, is a flagellated, binucleated, unicellular, eukaryotic, parasitic protozoan species that belongs to the *Giardia* genus and to the Zoomastigophorea class and the Diplomonadida order (Lane & Lloyd, 2002). This order is often characterized as a primitive, ancient protist group as it lacks typical eukaryotic organelles, such as mitochondria and peroxisomes, and possesses a poorly developed endomembrane system (Tovar et al., 2003). *Giardia* species are characterized based on their morphology, with four other known species within the *Giardia* genus, *G. agilis, G. muris, G. psittaci,* and *G. ardeae,* as well as an ongoing debate about a sixth species referred to as *G. microti* (Adam, 2001). These species infect mammals and other animals including amphibians, reptiles, and birds while the only species that also infects humans is *G. intestinalis* (Lane & Lloyd, 2002). For the purpose of this thesis, *G. intestinalis* will be referred to as "giardia" unless it is being compared to any of the other *Giardia* species where a clear distinction will be made.

1.2.2 Morphology and Cell Cycle

     The morphology of giardia is characterized by the two stages of its life cycle. The first stage is an actively multiplying trophozoite that is about 15 µm in length and 5-9 µm in width, is teardrop-shaped and possesses two nuclei of equal size at the anterior end (Lane & Lloyd, 2002). Trophozoites have two median bodies that make an adhesive disc made of microtubules. Giardia trophozoites are located in the small intestine of their host and are able to swim freely in the duodenum and ileum due to their four pairs of flagella, one anterior, two posterior, and one caudal pair (Lane & Lloyd, 2002). They are also able to attach to the intestinal epithelium via the contraction of their adhesive ventral disk. Trophozoites replicate by repeated binary division and

as they move through the colon, they become cysts in a process called encystation triggered by the exposure to bile salts or also possibly from cholesterol starvation (Lane & Lloyd, 2002; Marshall et al., 1997; Ortega & Adam, 1997).

Giardia cysts are 10-12 µm in length and are excreted by the host in their feces. Cysts can survive in food and water and can remain viable for several months under favorable conditions of temperature and humidity, such as water at 4-10 ˚C (Ortega & Adam, 1997). Excystation, the process by which a cyst becomes a trophozoite, is triggered by the acidic environment in the stomach of the host upon the ingestion of a cyst (Lane & Lloyd, 2002; Marshall et al., 1997). The ability of giardia cysts to readily exist in the environment and infect new hosts as well as the parasitic nature of the trophozoites result in giardia infections (Figure 1).

1.2.3 Different Giardia Species and Genotypes

Giardia can be subclassified into different species based purely on morphological differences of the median body. The morphological characteristics that were just described in the previous section are what specifically constitute *G. intestinalis* as a species. Adam (2001) reviewed the differences between *Giardia* species, indicating that *G. intestinalis* is pear-shaped and has two transverse claw-shaped median bodies; the median body of *G. agilis* is teardrop-shaped and the trophozoite is long and slender; *G. muris* is characterized by being a shorter and rounder trophozoite and has a small rounded median body; *G. psittaci* and *G. ardeae* can only be differentiated by electron microscopy; the proposed *G. microti* has been suggested on the mere basis of host specificity.

G. intestinalis can be further subcategorized into 8 different assemblages or genotypes (A-H) as reviewed by Fantinatti et al. (2016). These assemblages were identified by the quantitative comparison of giardia isolates and sequence comparisons that showed varying levels

of divergence between said sequences (Adam, 2001). Giardia assemblages infect various hosts. Assemblages A, B, and E are the only assemblages that have been shown to infect humans; assemblages C and D have been found in dogs; assemblage E, besides being found in humans has also been found in grazing or herd animals; F is found in cats; G is found in rats and mice; and H in seals (Fantinatti et al., 2016).

1.2.4 Anti-Giardia Drugs

There are multiple drugs that are used in the treatment of giardiasis, with 5-nitroimidazoles (secnidazole, ornidazole, tinidazole, and metronidazole) being the preferred choice, metronidazole more specifically. Some of the other drugs that are used to treat giardiasis are benzimidazoles (albendazole and mebendazole), the aminoglycoside paromomycin, the acridine quinacrine, furazolidone, nitazoxanide, and chloroquine (Mørch & Hanevik, 2020). Despite working to some extent, these drugs are not giardia-specific as shown by Mørch & Hanevik (2020).

These drugs are broadly used in the treatment of giardia infections despite the many issues that arise from their use that are ultimately harmful to the host. The first drawback is that many of these drugs are repurposed drugs that were developed to treat completely different pathogens and are now being used to treat giardiasis. 5-nitroimidazoles are broad-spectrum antimicrobials, indicating that they will not only target giardia but will also affect commensal gut bacteria, thus causing dysbiosis in the gut microbiome. Albendazole and mebendazole, for instance, are anti-helminthic drugs. Nitazoxanide is used to treat *Cryptosporidium*. Chloroquine is used against non-falciparum malaria and rheumatic disorders (Mørch & Hanevik, 2020).

The mechanism of action of these drugs in giardia is also not completely understood and they exhibit extremely varying numbers of efficacy. Mørch & Hanevik (2020), reviewed the

varying levels of efficacy and showed that secnidazole and ornidazole, for instance, are typically over 90% effective, while mebendazole efficacy ranged from 14-95%. Another issue is the fact that there are many reports of cases with high incidences of nitroimidazole refractory cases in giardiasis. Mørch & Hanevik (2020) use the term refractory instead of resistance as they explain that due to a lack of defined molecular resistance mechanisms in giardia, using the term resistance would be deemed incorrect. These issues make it clear that there is a need to find and/or develop effective and reliable giardia-specific drugs.

1.2.5 Potential Pathways for Drug Targeting

Oxygen concentrations in the small intestine and the stomach of humans are rather low. The oxygen concentration in air is 158 mm Hg as opposed to 38 mm Hg in the small intestine and 15 mm Hg at the stomach mucosa in humans (Leitsch et al., 2018). These are the environments that giardia colonizes and despite its 'anaerobe' classification, it is able to thrive under these circumstances. Therefore, giardia has been defined as a "microaerophilic" or "microaerotolerant" parasite. Nonetheless, giardia faces high oxidative stress as a result of active countermeasures of the host immune system such as the secretion of reactive oxygen species (ROS), such as hydrogen peroxide, and reactive nitrogen species (RNS), such as nitric oxide and peroxynitrite (Leitsch et al., 2018). Hindering the pathways that giardia implements to deter ROS and RNS stress would result in cytotoxic effects for the parasite, ultimately killing it and clearing the infection. Studying these specific pathways with the aim to target them, has the potential to allow for the proper identification and development of drugs that are not only effective but also giardia-specific.

1.3 Reactive Oxygen Species and Reactive Nitrogen Species

1.3.1 ROS and RNS

ROS and RNS are pro-oxidants/oxidants derived from oxygen and nitrogen. They are

defined as oxidative and nitrosative agents respectively and can be classified into two categories;

radicals and non-radicals as reviewed by Phaniendra et al. (2015). Radical species have at least

one unpaired electron in a molecular orbital. The presence of one unpaired electron allows

radicals to donate it or to obtain another electron to reach a more stable state in which all

electrons are paired, making them highly reactive. Examples of free radicals ROS and RNS

include superoxide ($O^{\bullet-}_2$), molecular oxygen (which is a biradical $O^{\bullet\bullet}_2$), hydroxyl radical ($OH^\bullet$),

alkoxy radical ($RO^\bullet$), peroxyl radical ($ROO^\bullet$), nitric oxide ($NO^\bullet$) and nitrogen dioxide ($NO^\bullet_2$)

(Phaniendra et al., 2015). Certain ROS and RNS are not radicals but are prone to participate in

reactions that lead to radical formation. Examples of non-radical ROS and RNS include

hydrogen peroxide (H_2O_2), hypochlorous acid (HOCl), hypobromous acid (HOBr), ozone (O_3),

singlet oxygen ($^1O_2$), nitrous acid (HNO_2), nitrosyl cation (NO^+), nitroxyl anion (NO^-),

dinitrogen trioxide (N_2O_3), dinitrogen tetraoxide (N_2O_4), nitronium cation (NO_2^+), organic

peroxides (ROOH), aldehydes (HCOR), and peroxynitrite ($ONOO^-$) (Phaniendra et al., 2015).

1.3.2 Formation and Effects of Some ROS & RNS

1.3.2.1 ROS. The most common and important biological ROS is the superoxide anion radical,

which is formed by enzymatic processes, autooxidation reactions, and non-enzymatic electron

transfer reactions that result in an electron being transferred to molecular oxygen (O_2).

Superoxide can act as a reducing agent, for example reducing complexes of Fe^{3+} to Fe^{2+}, and it

also acts as an oxidizing agent, for example oxidizing ascorbic acid to dehydroascorbic acid

(Phaniendra et al., 2015). Under physiological conditions, superoxide is present both in its

protonated ($HO_2^•$) and deprotonated ($O_2^{•-}$) states. Hydrogen peroxide is a non-radical species that is the least reactive molecule among ROS. It forms in a dismutation reaction that is catalyzed by superoxide dismutase (SOD) in which 2 molecules of protonated superoxide form one molecule of molecular oxygen (O_2) and one molecule of hydrogen peroxide (H_2O_2). It can also form from the two-electron reduction of oxygen in reactions catalyzed by certain oxidases. H_2O_2 is highly diffusible and can easily penetrate biological membranes, leading to DNA damage upon its reaction with transition metal ions *via* the production of the hydroxyl radical (Ozcan & Ogun, 2015; Phaniendra et al., 2015). This radical is formed during the reaction of superoxide and hydrogen peroxide. The hydroxyl radical is the most reactive and dangerous radical and can strongly react with both organic and inorganic molecules including DNA, proteins, lipids, and carbohydrates(Ozcan & Ogun, 2015; Phaniendra et al., 2015).

1.3.2.2 RNS. Nitric oxide is a small molecule generated from microbiological denitrification and from the conversion of L-arginine to L-citrulline by the different nitric oxide synthases (NOSs). The most well-known NOSs are the three mammalian isotypes, neuronal (nNOS), inducible (iNOS), and endothelial (eNOS), but these enzymes are found in other animals as well as certain bacteria (Mastronicola et al., 2016; Rehder, 2014). Nitric oxide ($NO^•$, commonly abbreviated as NO) is an uncharged lipophilic free radical, allowing it to diffuse through plasma membranes. Although it is not a very reactive free radical, it can react with other molecules such as oxygen, superoxide, and glutathione to yield highly reactive and toxic intermediates that alter protein and DNA oxidation states (Ozcan & Ogun, 2015).

For example, NO reacts with superoxide to form peroxynitrite ($ONOO^-$), a highly toxic and reactive species that can directly react with carbon dioxide (CO_2) to form the highly reactive nitroso peroxo carboxylate ($ONOOCO_2^-$) or peroxynitrous acid (ONOOH). Peroxynitrous acid

undergoes homolysis to form the hydroxyl radical and nitrogen dioxide, or it can rearrange to form $NO\bullet_3OONO^-$, which can oxidize lipids, methionine, and tyrosine residues in proteins and oxidize DNA to form nitroguanine (Phaniendra et al., 2015). Other reactions involving nitric oxide are the formation of nitrate (NO_3^-) and nitrite (NO_2^-) from the reaction with molecular oxygen. A one-electron oxidation of nitric oxide results in the formation of the nitrosonium cation (NO^+) and a one-electron reduction results in the formation of the nitroxyl anion (NO^-). Both of these ions can react with nitric oxide to form dinitrogen monoxide (N_2O) and a hydroxyl radical.

1.3.3 Giardia, ROS and RNS

The capability of giardia to withstand exposure to oxidative stress is limited, which results in oxidative damage to the organism despite its "microaerophilic" status. A study by Lloyd et al. (2000) demonstrated oxidative damage to giardia trophozoites including damage to the electron transport systems responsible for O_2 reduction, as well as a wide range of damage to cellular functions. More specifically, oxygen and its reaction products damage the plasma membrane of giardia cells, leading to swelling of the organism and the loss of the regulatory volume control process (Lloyd et al., 2000).

Among the sites that are known to be inhibited by molecular oxygen in giardia, are the (4Fe-4S) iron-sulfur cluster of ferredoxins, a class of electron transport proteins (Ellis et al., 1993). The article by Lloyd et al. (2000) also discusses how inhibition can also be immediately replicated when the cells are exposed to 60 μM hydrogen peroxide, suggesting that exposure to inhibitory levels of molecular oxygen causes the accumulation of the partially reduced hydrogen peroxide byproduct. Hydrogen peroxide then reacts with superoxide to produce the hydroxyl radical, which is suspected to be an important intracellular oxidant as supported by experiments

dealing with a loss of functional activity that is reverted in the presence of hydroxyl radical scavengers (Lloyd et al., 2000).

Giardia is also affected by nitrosative stress as a result of nitric oxide that is produced by host iNOS or through nitrite reduction. More specifically, the formation of peroxynitrite caused by the reaction of nitric oxide and superoxide causes harmful effects on giardia cells including the deamination of nucleotides and the irreversible inhibition of metalloenzymes (Leitsch et al., 2018). A study performed by Mastronicola et al. (2016) dealt with the effect of different nitrosative stressors (S-nitroso-acetyl-penicillamine, sodium nitroprusside, and nitrite) on giardia trophozoites. They found that such nitrosative stressors displayed cytotoxic effects against trophozoites, including inducing the loss of plasma membrane potential, morphological alterations, reduced ability to consume oxygen, reduced flagellar motility, higher susceptibility to osmotic stress, and cell death.

1.3.4 Protection Against Oxidative and Nitrosative Stress in Giardia

In most eukaryotes, ROS detoxification is multilayered and involves several enzymes including superoxide dismutase, catalase, peroxidase, glutathione reductase, plus the reducing agent glutathione (Brown et al., 1995; Li & Wang, 2006). Although it is a eukaryote, giardia does not possess any of these commonly used enzymes and agents, suggesting that as a microaerophilic parasite, it must have alternative enzymes and pathways to deal with oxidative stress. Several studies regarding giardia's antioxidant and antinitrosative defense systems have been performed that have allowed for the identification and characterization of different enzymes that this eukaryote possesses and allow it to protect itself from ROS and RNS.

The main known enzymes involved in ROS detoxification in giardia are a membrane-associated NADH-peroxidase (Brown et al., 1995), a DT-diaphorase (Li & Wang, 2006), a

superoxide reductase (SOR) (Testa et al., 2011), an NADH-oxidase (Brown et al., 1995, 1996), a flavodiiron protein (Di Matteo et al., 2008), as well as two peroxiredoxins (Mastronicola et al., 2014), and a flavohemoglobin (Rafferty & Dayer, 2015). The peroxiredoxins, flavodiiron protein, and flavohemoglobin of Giardia also play roles in RNS detoxification. Amongst the enzymes found in giardia that act as both RNS and ROS defenses, the flavohemoglobin is of particular interest as it contains the heme cofactor and giardia lacks the required pathways for heme biosynthesis (Rafferty et al., 2010).

1.4 Flavohemoglobins

Flavohemoglobins (FlHbs) are fusions of an amino-terminal, heme-containing globin domain and a carboxy-terminal flavin adenine dinucleotide-containing domain (Figure 2) that belongs to a family of proteins called ferredoxin nucleotide reductases (FNR). Although the globin domain of flavohemoglobins is homologous to that of globins involved in oxygen transport and storage, the residues within the heme pocket promote oxygen activation for subsequent reactions instead of promoting reversible oxygen binding as seen in oxygen-carrying globins. FlHbs play a major role in nitrosative defense because of their nitric oxide dioxygenase (NOD) activity, and can also act as NAD(P)H oxidases, reducing O_2 to water in the absence of nitric oxide (Rafferty & Dayer, 2015).

FlHbs are an efficient defense against RNS and there are many different flavohemoglobin isotypes widely distributed among microorganisms. Sequences for FlHbs are some of the most abundant globin genes in bacteria, with over 530 sequences being reported. A newer survey conducted by Poole (2020) indicates that there are 3,318 flavohemoglobin sequences, with 2,363 being bacterial FlHbs and 204 being eukaryotic. Bacterial FlHb sequences are distributed across 10 bacterial divisions with most of them found in Proteobacteria, while they are uncommon in

other divisions such as Bacteroidetes and Cyanobacteria. Eukaryotic FlHbs are found in yeast, ameoba, and certain protozoans, including giardia. Poole suggests that flavohemoglobins arose in bacteria from an ancient globin, and it is possible that flavohemoglobins spread to eukaryotes through horizontal gene transfer. Even though such transfers between the domains of life are infrequent in biology, "single-protein metabolic modules" such as flavohemoglobins are prone to gene duplication, and therefore horizontal gene transfer during evolution.
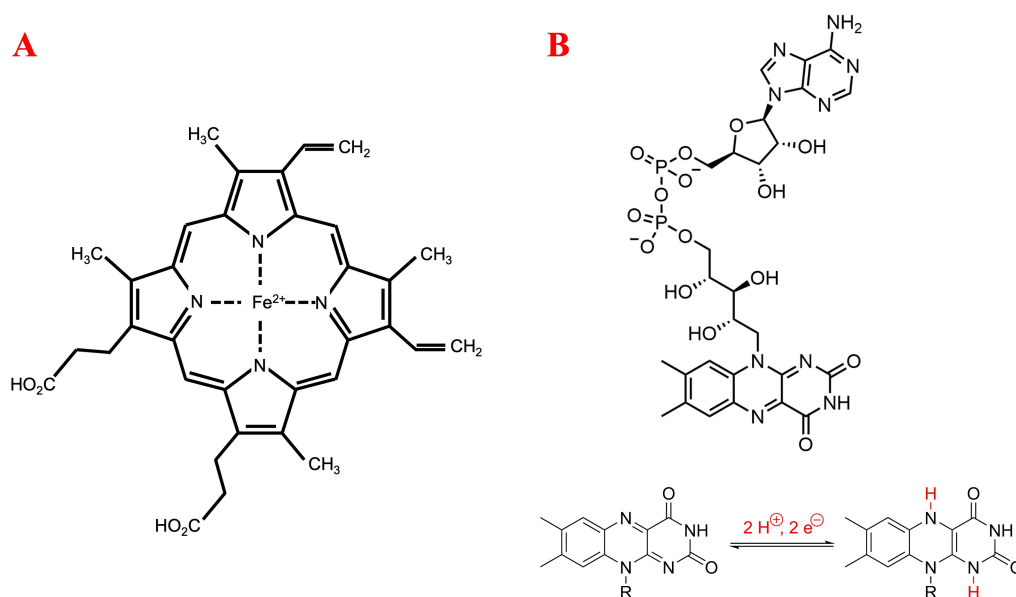
Figure 2: Structures of heme and FAD. A) Structure of heme. B) Structure of FAD, displaying the fully oxidized and fully reduced isoalloxazine rings in the bottom. Taken from Wikipedia, free use.

1.4.1 The Heme Cofactor

Iron is a redox-active metal of great biological importance. As iron has multiple stable oxidations states such as Fe^{2+} and Fe^{3+}, iron complexes are a major component of biological electron transfer chains. Iron cations can also act as electron pair acceptors and bind to ligands that are electron pair donors to form a variety of coordination complexes, and it has high flexibility related to the nature of ligand it binds and coordination geometry of the resulting

metal-ligand complexes (Rehder, 2014). These complexes are integral molecular or ionic units that possess a metal ion bonded to a specific number of ligands in a specific geometrical arrangement such as in heme.

The ligands in coordination compounds or complexes can be ions (simple or composite) or molecular dipoles. Metal-ligand coordination can be described in terms of Lewis acid/Lewis base interactions where each ligand provides a free electron pair (Lewis base) while the metal in the coordination centre is the Lewis acid. This interaction can also be defined in terms related to bonding, as denoted in L→M, where L refers to the ligand (electron pair donor), → refers to the bonding electron pair, and M refers to the metal (the electron pair acceptor). A coordination complex tends to be more stable when the overall electron configuration is 18 for transition metals such as iron, including the sum of the metal's valence electrons and electron pairs from the ligands (Rehder, 2014).

The iron-containing prosthetic group of FlHbs is heme B, which comprises a coordination complex between ferrous (Fe^{2+}) or ferric (Fe^{3+}) ion and the porphyrin ring of poroporphyrin IX (Figure 2). The porphyrin ring consists of four five-membered pyrrole rings bridged by four methyne carbons and has the metal ion coordinated to each nitrogen of the four pyrrole rings. From this point onwards, heme B will be referred to simply as heme. In heme, iron has a coordination number of four and has a square planar geometry, but the heme iron can accommodate up to two more ligands to form five-coordinate square planar complexes or six-coordinate octahedral complexes. When bound to a protein, amino acid side chains from the protein will provide one or two of these additional ligands called the axial ligands, as their metal-ligand bonds are at right angles to four metal-ligand bonds formed by iron and the porphyrin. Histidine, cysteine and tyrosine are common axial ligands. If the protein provides only one

additional ligand, the remaining coordination site can be taken by O_2, which can bind to Fe^{2+} heme. In oxygen-binding heme proteins the face of the heme where oxygen binds is called the proximal side, and the opposite face is called the distal side.

Heme is a relatively nonpolar molecule and it is mostly or totally buried within the hydrophobic interior of the protein. In globins, it is embedded in a hydrophobic crevice formed by six alpha helixes, which allows the formation of extensive van der Waals contacts with adjacent polar residues as well as axial ligation to a histidine side chain. In the case of FlHbs, this proximal histidine is hydrogen-bonded to an adjacent glutamate residue, which increases the electronegativity of the histidine and promotes activation of oxygen for subsequent reaction rather than reversible oxygen binding (Mukai et al., 2001). Another major difference between the oxygen transport globins and the globin domain of flavohemoglobins is the existence of a distal histidine residue in the former and its absence in the latter. In oxygen transport globins, such as in hemoglobin, oxygen coordinates to ferrous iron into the axial position opposite to the proximal histidine residue. Heme then adopts a 'bent' orientation that is further stabilized by hydrogen bonding interaction with the distal histidine residue, more specifically by interacting with the NH group of the imidazole side chain. In this context, when oxygen binds heme, the iron ion is oxidized by O_2 to form a ferric superoxide complex. In the oxygen transport proteins this is reversible and O_2 is released, resulting in no net change in the oxidation state of the iron (Rehder, 2014).

Bacterial FlHbs, on the other hand, lack the distal histidine residue required to hydrogen bond molecular oxygen. Instead, they have a leucine residue and nearby hydrogen-bonding tyrosine and glutamine residues (Rafferty & Dayer, 2015). Nonetheless, these residues serve a purpose similar to that seen in the distal histidine residue in oxygen-transporting globins as

explained by Bonamore & Boffi (2008). They suggest that the distal tyrosine and glutamine residues are involved in the stabilization of molecular oxygen when it binds to the iron in heme for subsequent reaction rather than reversible binding.

1.4.2 The FAD-Containing Domain

The role of the flavin adenine dinucleotide (FAD) cofactor within FlHbs is to act as an electron carrier. FAD acts as the electron carrier from NAD(P)H to the ferric heme prosthetic group, thus restoring it to the ferrous state (Gardner et al., 1998). This reaction occurs due to the electronic linkage of flavin and heme. FAD is reduced to leukoflavin by NAD(P)H and the ferric iron in heme is reduced by the FAD hydroquinone and semiquinone univalently and sequentially (Gardner et al., 1998). The electron transfer from NAD(P)H to the heme prosthetic group mediated by FAD is what allows for the catalytic NOD cycle of FlHbs to reset after each redox reaction.

The fold of the FAD-containing domain corresponds to the overall architecture of the ferredoxin reductase (FNR-like) family and can be further subcategorized into two domains, the two subdivisions being the FAD-binding domain and the NAD-binding domain. The FAD-binding domain consists of a six-stranded antiparallel **β**-barrel with Greek key topology capped by a helix at the bottom and an irregular peptide segment connecting two of the strands at the top while the NAD-binding domain is made of a five-stranded parallel **β**-sheet flanked by two helixes on one side and by a helix and an irregular peptide segment on the other side (Ermler et al., 1995). These two domains are fused to build an oxidoreductase module that belongs to the ferredoxin reductase family. The oxidoreductase module plays a vital role in the transfer of electrons that takes place within the flavohemoglobin and allows it to perform its catalytic duties.

The FAD-binding pocket in flavohemoglobins positions the redox-active isoalloxazine ring of the cofactor 10-12 Å from the heme iron. The residues of the FAD-binding pocket vary according to the flavohemoglobin isotype but most of the contacts are well conserved and exhibit identical orientations with respect to the isoalloxazine plane. The main differences between isotypes within this domain seem to be related to the relative orientation of the two subdomains that lead to considerable changes in the interdomain cleft of the flavohemoglobin and its binding interactions with phospholipid molecules (Bonamore & Boffi, 2008).

1.4.3 Nitric Oxide Dioxygenase Activity

FlHbs play a vital role in battling nitrosative stress by acting as nitric oxide dioxygenases (NOD). This enzymatic function is characterized by the conversion of NO and O_2 to innocuous nitrate (NO_3^-) (Figure 3) (Gardner et al., 1998). In the absence of the enzyme, the oxidation of NO in aqueous conditions yields nitrite (NO_2^-) (Ignarro et al., 1993). FlHbs are efficient NODs and require the involvement of molecular oxygen as a co-substrate as well as nicotinamide adenine dinucleotide (NADH) or nicotinamide adenine dinucleotide phosphate (NADPH) and FAD as cofactors for the catalytic cycle.

The NOD mechanism in FlHbs involves two steps after the Fe^{2+} in heme binds O_2, which as in the case of hemoglobin forms a ferric superoxide complex, $Fe^{3+}\text{-}O_2^{\bullet-}$ (Figure 3). The first step consists of the rapid reaction of NO with the $Fe^{3+}\text{-}O_2^{\bullet-}$ intermediate to form a ferric peroxynitrite complex, $Fe^{3+}\text{-}OONO$. The second step involves the rapid isomerization of the intermediate to form nitrate NO_3^- which is thought to proceed through a pathway where the O-O bond homolyzes to form a $[Fe^{4+}=O/\,^{\bullet}NO_2]$ intermediate before the oxyferryl oxygen attacks $^{\bullet}NO_2$ to form nitrate (Poole, 2020). As this leaves the iron in the ferric (Fe^{3+}) state, to be able to complete another catalytic cycle, a one-electron reduction is required to regenerate ferrous iron

(Fe^{2+}) in heme (Poole, 2020). Here, either NADH or NADPH serve as the ultimate electron donors, although flavohemoglobins preferentially use the former.

The NADH and NADPH cofactors are obligate 2-electron donors and since the iron ion in heme requires a single electron, the transfer of electrons must take place through FAD as it is able to accept electrons in pairs and donate them singly (Rafferty & Dayer, 2015). This transfer of electrons occurs as NADH reduces FAD to leukoflavin. Once the FAD is reduced, the Fe^{3+} in heme is reduced to Fe^{2+} by the FAD's hydroquinone and semiquinone univalently and sequentially. Once this transfer of electrons is complete and the iron in heme is back in its ferrous state, a new catalytic cycle can rapidly occur (Gardner et al., 1998).
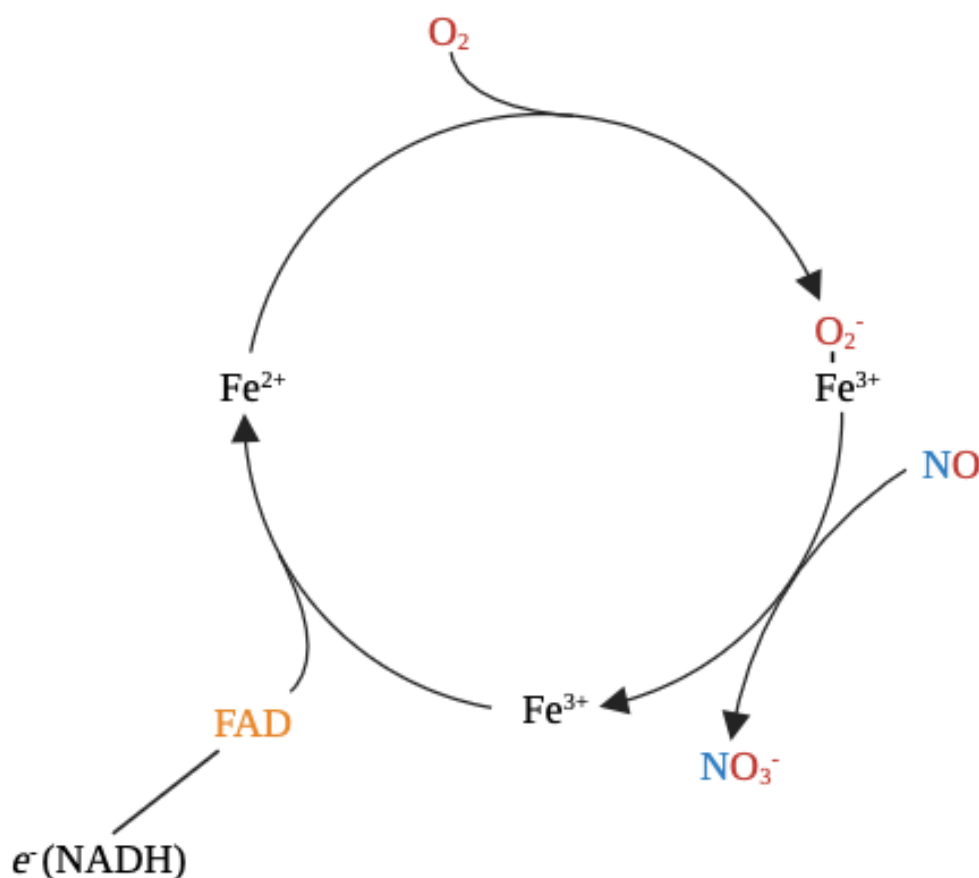
Figure 3: *The catalytic cycle for NOD activity of FlHbs. Heme is represented by the Iron. The electron may come from NADH as shown in the figure or NADPH. Created using BioRender.*

1.4.4 Giardia Flavohemoglobin

The FlHb of giardia (gFlHb) acts as a NOD (Figure 3) and in the absence of NO it also exhibits NADH oxidase activity, by reducing O_2 to water, protecting the parasite from stress induced by both ROS and RNS (Rafferty & Dayer, 2015). Its NOD activity follows the pathway described above, using NADH and FAD as cofactors (Mastronicola et al., 2010; S. Rafferty et al., 2010; Rafferty & Dayer, 2015). To date, there are no crystallographic studies that have been performed on gFlHb to determine its structure. However, as the sequence of gFlHb is about 40% identical to that of the flavohemoglobin found in *Escherichia coli* (Hmp), and whose structure was determined by x-ray diffraction (Ilari & Boffi, 2008). The similarity between the sequences of Hmp and gFlHb has allowed researchers to use the known structure of Hmp as a template for the construction of homology model structures of gFlHb (Rafferty & Dayer, 2015) as well as more recent modelling using Alphafold (Jumper et al., 2021). The residues found in the cofactor binding regions of gFlHb and Hmp are well conserved with a proximal histidine-107 ligand (residues numbered according to the gFlHb sequence) that is hydrogen-bonded to the adjacent glutamate-157 increasing the electronegativity of the histidine, clearly distinguishing these globins from the ones that can reversibly bind oxygen (Mukai et al., 2001; Rafferty & Dayer, 2015). The distal faces of gFlHb and Hmp have a leucine-58 residue and nearby hydrogen-bonding residues tyrosine-30 and glutamine-54. These residues make gFlHb and Hmp different from oxygen-transporting globins as in place of these residues, oxygen-carrying globins have a distal histidine residue that is used to hydrogen bond oxygen (Rafferty & Dayer, 2015).

Although gFlHb and Hmp share a high degree of sequence and inferred structural similarity, there is a feature that gFlHb possesses that distinguishes it from any other FlHb: gFlHb has two sequence inserts that are not found in any other member of this enzyme class

(Figure 4). Each one of these inserts is approximately 25 amino acid residues long and one is located in each of the globin and FNR domains. The globin domain inserts are located between residues 75 and 98 while the ones in the FNR domain are found between residues 280 and 307 (Rafferty & Dayer, 2015). Homology modelling and Alphafold predict that these inserts are in contact with each other and that they may contribute to forming tighter interactions between the globin and FNR domains of gFlHb based on their size and location within the enzyme.
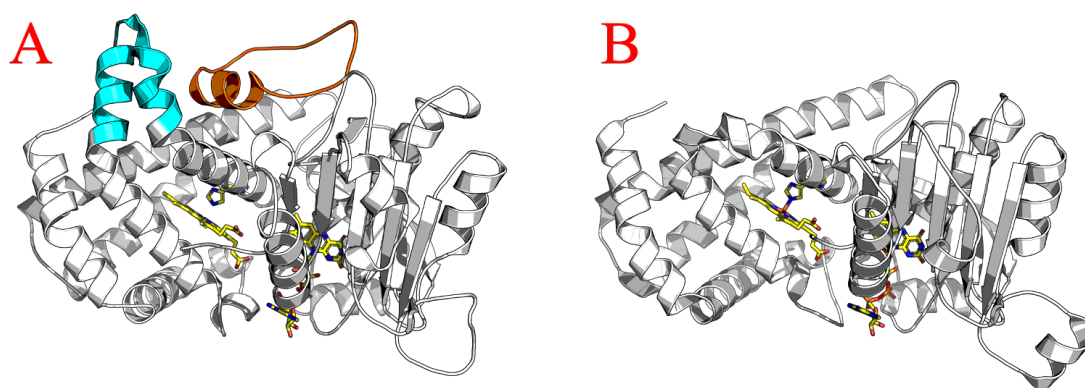
Figure 4: Ribbon structures of FlHbs. Heme, FAD, and the proximal His ligand are in yellow. *A)* Homology model of gFlHb (52 kDa) constructed using Alphafill, showing the position of the unique inserts (cyan: residues 75-98; orange: residues 280-307). *B)* Structure of E. coli Hmp (44 kDa; 1gvh.pdb)

The structural and genetic similarities between gFlHb and Hmp, as well as their structural differences, more specifically the presence of the additional sequence inserts in gFlHb, make these two enzymes a good starting point to compare the function and behavior of FlHbs. The differences amongst flavohemoglobin isotypes pose an opportunity to study how these different microorganisms combat nitrosative stress. By understanding how their NOD activity differs or how their structural differences affect them, the possibility to develop treatments that exhibit isotype selectivity to only fight off the unwanted harmful microorganisms arises. The broad range of bacterial divisions that possess flavohemoglobin sequences also includes bacteria that are commensals to their hosts and that would cause more harm than good if eradicated from the

host's microbiome, such as *E. coli.* Studying how different isotypes behave may allow scientists to target treatment plans more specifically. Inhibiting gFlHb might help the host's immune system get rid of giardia by promoting the formation of RNS within the GI tract and ultimately triggering cytotoxic effects.

1.4.5 Inhibiting FlHbs

Inhibitors that are able to target the heme prosthetic group of FlHbs are potentially good candidates for antibiotic development as described by Helmick et al. (2005), who suggested that the NOD activity of FlHbs could be inhibited by a ligand that is able to coordinate the catalytic heme iron and fit within the large hydrophobic distal heme pocket. They also noted that ligands, such as imidazole-based drugs that contain bulky aromatic substituents offer the potential for selective inhibition of NOD activity. Helmick et al. (2005) tested this by performing kinetic studies on Hmp where they used varying concentrations of different ligands to study their effect on Hmp's NOD activity. Their research showed that imidazole-based drugs were able to inhibit microbial NOD activity, more specifically miconazole, econazole, clotrimazole, and ketoconazole with respective K_i values of 80; 550; 1,300; and 5,000 nM, respectively.

Crystallographic studies that have been performed on Hmp and FHP (*Alcaligenes eutrophus* FlHb) have allowed scientists to identify that FlHbs possess large hydrophobic heme pockets that are capable of sequestering bulky aliphatic lipids and imidazole N-1 substituents (Helmick et al., 2005; Ilari et al., 2002; Ollesch et al., 1999). The affinity of heme pockets for lipids correlates well with the ability of large hydrophobic imidazoles to inhibit NODs (Vanden Bossche et al., 2003). The research performed by Helmick et al. (2005) revealed that imidazole binding prevents the NADH-mediated reduction of heme and FAD. As it was explained in section 1.4.3, NOD activity requires the reduction of the ferric heme via an electron shuttle from

free NADH to bound FAD to the heme. Helmick et al. (2005) were able to observe a slower rate of transition from the ferric to the ferrous state with miconazole coordination indicating that coordination of miconazole to the ferric heme iron inhibited heme and FAD reduction in Hmp.

The results from the research performed by Helmick et al. (2005) confirm that ligands with bulky aromatic substituents can inhibit Hmp by coordinating the heme iron within the heme pocket. Their study also looked at FHP, which has a higher affinity for lipids than Hmp (Ollesch et al., 1999), and allowed them to correlate the ability of large hydrophobic imidazoles with the ability of heme pockets for lipids: *A. eutrophus > E. coli.* These isotypic differences as well as the evidence obtained from the studies confirm that not only are imidazole-based ligands good candidates for antimicrobials that inhibit NODs but that they interact differently with different FlHbs isotypes. Considering the high similarity between the sequences of gFlHb and Hmp, as well as the major differences between the structures of these isotypes, especially around the hydrophobic heme pocket, studies that focus on the screening of gFlHb should focus on testing imidazole-based inhibitors. The evidence suggests that based on the ability of imidazole-based ligands to inhibit Hmp, they also have the potential to inhibit gFlHb. Nonetheless, their specific activities and interactions with the active site of gFlHb might differ from that of Hmp based on the differences in the enzymes' heme pockets.

1.5 Screening for gFlHb Inhibitors

As with Hmp, the efficacy of inhibitors of gFlHb would be measured in terms of how effective the compounds are in inhibiting the enzyme's NOD activity. Imidazole-based ligands have the potential of successfully inhibiting gFlHb given their interference with the NADH-mediated reduction of heme. Nonetheless, there are many imidazole-based drugs that have the potential to inhibit these enzymes besides the ones that have already been shown to inhibit Hmp.

The high number of compounds that could inhibit either one of the two enzymes requires the development of a high-throughput screening method that is rapid, cheap, and effective and that can not only tell whether a compound is a good inhibitor or not but also whether a compound displays isotype selectivity as the ultimate goal would be the sole inhibition of gFlHb to preserve commensal gut bacteria while eradicating the parasite.

The inhibition of gFlHb be studied by measuring the enzyme's NOD activity. The NOD activity depicted in Figure 3 catalyzes the conversion of NO to nitrate, NO_3^-, by FlHbs. In the absence of these enzymes, such NOD activity is not seen and instead, the principal oxidation product of NO in aerated or oxygenated environments is nitrite, NO_2^- (Ignarro et al., 1993). This clear difference in the oxidation products of NO allows for the study of FlHb inhibition. In a controlled reaction, with known concentrations of nitric oxide donors, the effectiveness of an inhibitor can be assessed by measuring the concentration of nitrite that is present in the solution once the enzyme-catalyzed reaction is over. A successful inhibitor would yield high nitrite concentrations as opposed to the low nitrite values that would be seen if the enzyme is not inhibited as nitrate is formed. This difference in NO oxidation products between enzyme-catalyzed and uncatalyzed processes is the basis for studying gFlHb inhibition by imidazole-based ligands rapidly and effectively.

1.5.1 The Griess Assay

Several methods for the quantification of nitrite are available that differ in principle of detection and the instrumentation required (Nam et al., 2018). These include capillary electrophoretic, chemiluminescent, fluorescent, electrochemical, and high-performance liquid chromatographic methods (Nam et al., 2018). One attractive option that is low-cost, portable, and allows rapid detection of nitrite is the colorimetric Griess assay (Nam et al., 2018).

The Griess assay is the oldest, most well-known, and most frequently used method of analysis of nitrite and nitrate and is based on the Griess reaction (Griess, 1879). The original reaction was developed by the German chemist Johann Peter Griess (1829-1888) and involved the synthesis of the azo dye "diazobenzolamidonaphtol" from napthylamine and diazobenzene, which would be replaced by diazobenzene sulfonic acid, in order to increase the water-solubility of the azo dye (Griess, 1879). In this original reaction, nitrite ions react with sulfanilic acid under acidic conditions to yield a diazonium ion; the diazonium ion then couples to **α**-naphthylamine producing a water-soluble, reddish-colored azo dye.

The Griess reaction that is known today differs from the original one, as it now relies on sulfanilamide and *N*-(1-naphthyl)ethylenediamine (NED). NED is a better coupling agent for sulfanilamide over other compounds, such as 1-naphthylamine, as it allows for more reproducibility, faster coupling, increased sensitivity, and acid-solubility of the azo dye (Tsikas, 2007). In this method, nitrite is treated with a diazotizing reagent (sulfanilamide) in acidic media to form a diazonium salt, which then reacts with a coupling reagent (NED) to form a stable azo compound (Figure 5) (Sun et al., 2003). The absorbance of the resulting azo compound can be measured between 540 nm to 550 nm and is linearly proportional to the concentration of nitrite in the sample (Misko et al., 1993; Sun et al., 2003; Tsikas, 2007). The two-step nature of the diazotization Griess reaction allows for variation among procedures where the order of addition of the Griess reagents (NED and sulfanilamide) changes. Sulfanilamide and NED can be pre-mixed in acidic media prior to their reaction with nitrite, or NED can be added after allowing nitrite and sulfanilamide to react in an acidic medium (Sun et al., 2003).
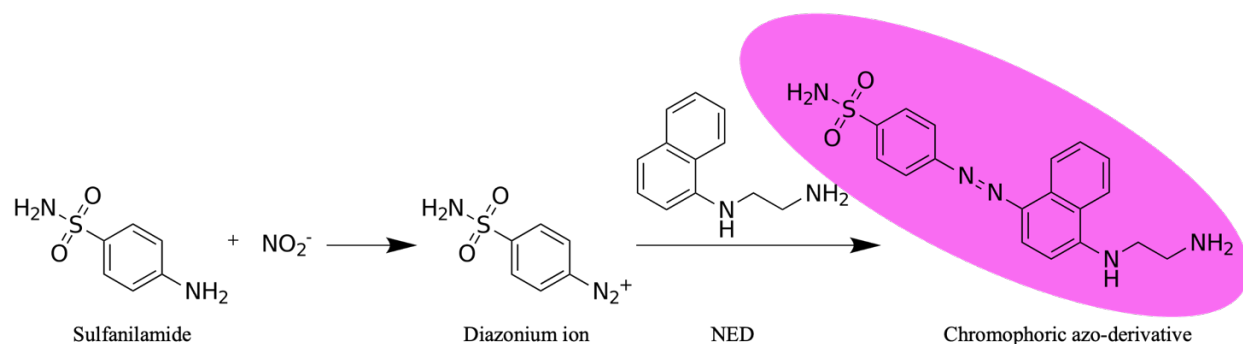
Figure 5: *The steps in the Griess reaction that produces a chromophoric azo-derivative (pink) that can be measured at 550 nm. Taken from Wikipedia, free use.*

This assay has the potential to be used for the screening of FlHb inhibitors. The two-step diazotization Griess reaction allows for a low-cost, rapid detection of nitrite in a sample (Figure 5). Successfully inhibiting the NOD activity of FlHbs would cause higher levels of nitrite to be present in the sample owing to uncatalyzed oxidation of NO to nitrite. Nitrite would then interact with the Griess reagents to form the azo dye that can be measured through its absorbance (Figure 5). Screening for inhibitors for a particular enzyme is an arduous process that involves the testing of many different ligands and a broad range of concentrations for each compound. Testing inhibitors can easily become an expensive and tedious task if it is performed on instruments such as high-performance liquid chromatography systems. The Griess assay, when performed on a microtiter 96-well plate, has the potential to test various ligands, different concentrations of these compounds, and even different FlHbs in one single experiment. Even in the absence of a microplate reader or a spectrophotometer, the azo dye that is formed during the Griess reaction is visible to the naked eye, allowing whoever is performing the assay to visualize the success or lack thereof for a particular inhibitor (Figure 6).
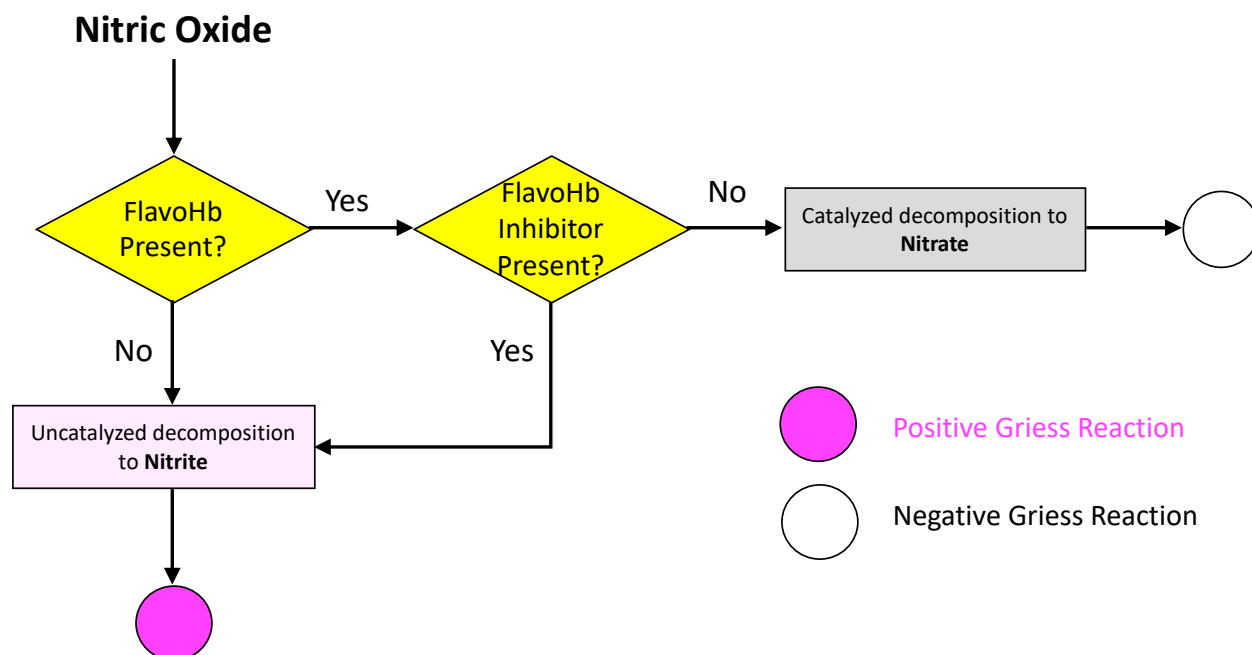
Figure 6: *Flow chart that shows the possible outcomes for the Griess assay when performed on FlHb (referred to on the chart as FlavoHb).*

1.5.2 Fluorescence Assay for Nitrite Based on 2,3-diaminonaphthalene

Misko et al. (1993) developed a rapid and sensitive fluorometric assay for nitrite adapted from a method proposed by Damiani & Burini (1986), and found that this fluorometric assay is 50-100 times more sensitive than the Griess assay. This assay was developed for the quantification of nitrite based on the changes in fluorescence of the fluorescent probe 2,3-diaminonaphthalene (DAN). This fluorescence assay combines speed and sensitivity when handling a large number of samples as they adapted it to a 96-well plate format for the quantification of nitrite from *in vitro* and *in vivo* sources.

DAN reacts with nitrite under acidic conditions, similarly to sulfanilamide in the Griess assay, and forms the fluorescent product 1-*(H)*-naphthotriazole or naphthalenetriazole (NAT) (Figure 7). Upon the addition of the fluorescent probe to the system and a ten-minute incubation time, a base such as sodium hydroxide (NaOH) is added to quench the reaction and allow for the

formation of the fluorescent product. The DAN reagent is prepared in hydrochloric acid to ensure

the acidic conditions required for the reaction to take place and must be mixed immediately with

the sample. It is also important to keep the DAN reagent away from light as it is sensitive to it as

well as only using DAN that has been prepared freshly over the last six months (Misko et al.,

1993). Fluorescence excitation and emission spectra of NAT are 365 nm and 450 nm

respectively.

The DAN fluorescence assay is much more sensitive than the Griess assay and can

measure nitrite concentrations in the low micromolar range (1-5 µM) which is ideal for the

screening of FlHbs inhibitors as it would detect even the slightest differences between two nitrite

samples. The results from this assay are also linearly proportional to the concentration of nitrite

in the sample allowing for a rapid and accurate analysis.
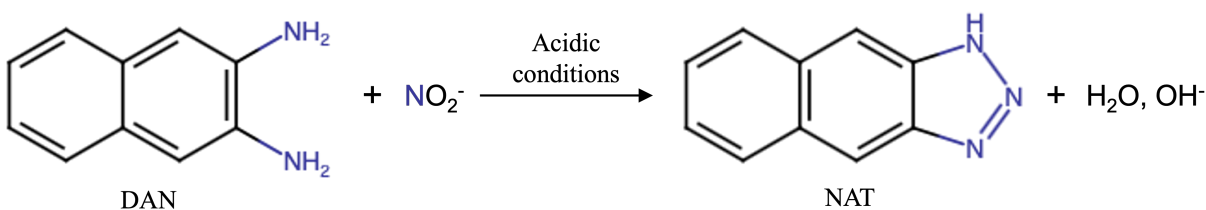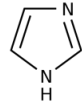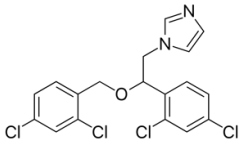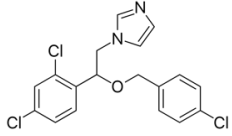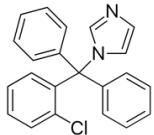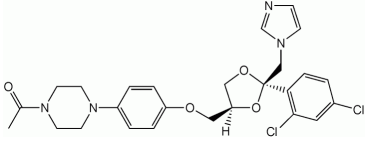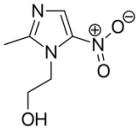
Figure 7: Reaction between 2,3-diaminonaphthalene and nitrite in acidic conditions, yielding the fluorescent product naphthalenetriazole (NAT), water, and a hydroxide ion.

1.6 Thesis Aims

The first objective of this research is to develop high-throughput assays to screen for

FlHbs inhibitors by using absorbance and fluorescence measurements on a 96-well microplate

format. As FlHbs catalyze the oxidation of NO to nitrate, their inhibition would instead result in

the uncatalyzed oxidation of NO of nitrite, which could be detected either spectrophotometrically

with the Griess assay or fluorometrically with the DAN assay. The optimization of the experimental conditions to develop these assays for detection of FlHb inhibition are described here.

Table 1: Properties of ligands used in this work.

Ligand	Formula	Molar Mass (g/mol)	Structure
Imidazole	$C_3N_2H_4$	68.08	
Miconazole	$C_{18}H_{14}Cl_4N_2O$	416.13	
Econazole	$C_{18}H_{15}Cl_3N_2O$	381.68	
Clotrimazole	$C_{22}H_{17}ClN_2$	344.84	
Ketoconazole	$C_{26}H_{28}Cl_2N_4O_4$	531.43	
Metronidazole	$C_6H_9N_3O_3$	171.16	

The second objective of this research is to test a group of imidazole-based drugs (Table 1) on both gFlHb and Hmp, using the Griess and fluorescence assays described in this thesis, to assess the different effects of inhibitors on these different isotypes. Hmp has been shown to be inhibited by imidazole-based drugs (Helmick et al., 2005) but there are no such studies

performed on gFlHb. This comparison would allow for a better understanding of how structural differences affect an isotype's interaction with a specific ligand, given the unique sequence inserts in gFlHb (Figure 4) (Rafferty & Dayer, 2015).

Lastly, this research could lead to the development of inhibitors that display isotype selectivity. Ideally, inhibitors would only target the NOD activity of gFlHb, allowing for the survival of *E. coli,* a commensal gut microorganism that coinhabits the gastrointestinal tract along with giardia. The high sensitivity of the Griess and fluorescence assays has the potential of displaying isotype selectivity, which can then be used to develop gFlHb-specific ligands to be used in the treatment of giardiasis.

2. MATERIALS AND METHODS

2.1 Protein Expression and Purification

2.1.1 Protein Expression

Recombinant protein expression and purification were conducted using the same methods for gFlHb and Hmp. Both enzymes were expressed recombinantly in the vector pET14b, which encodes an N-terminal hexahistidine tag for purification by immobilized metal affinity chromatography and which confers ampicillin resistance. The vectors were transformed into BL21(DE3) competent *E. coli* cells (New England Biolabs). This was done by adding 1-5 µL containing 1-100 ng of plasmid DNA directly to a vial containing 50 µL of competent cells, that had been thawed and kept on ice for 10 minutes, immediately followed by flicking the tube 4-5 times to mix the cells and the plasmid DNA. The mixture containing the cells was then placed on ice for 30 minutes, after which it was heat shocked at 42°C for 10 seconds and placed on ice for 5 minutes to allow the cells to recover. A 950 µL aliquot of room temperature SOC media (New England Biolabs) was added to the mixture and mixed by flicking the tube 4-5 times and inverting it. The cell mixture was then placed in a shaker incubator (VWR 10 L Shaker Incubator) at 37°C and 250 rpm for 60 minutes. 20 µL of the recovered cells were plated onto an LB Miller (BioShop Life Science Products) Agar plate with ampicillin (100 µg/µL) and incubated overnight at 37°C.

The next day, a single colony of the plate of bacteria was obtained to inoculate 2 mL of LB Miller media supplemented with ampicillin (100 µg/µL). The culture was then incubated in a shaker incubator (VWR 10 L Shaker Incubator) at 37°C and 250 rpm for 24 hours, after which the liquid culture was mixed with an equal volume of 50% glycerol, ~2 mL (for a final glycerol

concentration of 25%) for the preparation of frozen glycerol stocks. The cell mixture containing

the glycerol was then divided into 100 µL aliquots, which were stored in the freezer at -80˚C.

For protein expression, an aliquot of thawed transformed competent cells was transferred

to a culture tube containing 2 mL of LB Miller media supplemented with ampicillin (100 µg/µL).

Multiple culture tubes were prepared for each gFlHb and Hmp and were then incubated at 37˚C

and 250 rpm overnight. Next, the cultures were used to inoculate 2 L Erlenmeyer culture flasks

containing 500 mL of LB Miller media and supplemented with the following lactose-driven

autoinduction supplements: lactose, glycerol, trace metals, glucose, magnesium sue ($MgSO_4$),

ampicillin, 5-aminolevulinic acid (ALA), iron (III) chloride ($FeCl_3$), and calcium chloride

($CaCl_2$) (Table 2).

Table 2: *Lactose-driven autoinduction media used for protein expression. * 100x Trace Metals contains 10 µM*
$MnCl_2 \cdot 4H_2O$, 10 µM $ZnSO_4 \cdot 7H_2O$, 2 µM $CoSO_4 \cdot H_2O$, 2 µM $CuSO_4 \cdot 5H_2O$, 2 µM $NiSO_4 \cdot 6H_2O$, and 2 µM H_3BO_3.

Component	Per 100 mL LB
gFlHb/Hmp Culture	1 mL
10% Lactose	2 mL
50% Glycerol	1 mL
100x Trace Metals*	1 mL
20% Glucose	250 µL
1.0 M $MgSO_4$	200 µL
100 mg/mL Ampicillin	100 µL
100 mM ALA	100 µL
100 mM $FeCl_3$	50 µL
100 mM $CaCl_2$	20 µL

The flask necks were tightly covered with tinfoil and were then incubated in a shaker

incubator (VWR 10 L Shaker Incubator) for 20-24 hours at 37˚C and 250 rpm. Cultures were

poured into 50 mL Falcon tubes, and the cells were pelleted at 9,000 g (7,470 rpm) and 4˚C for

30 minutes, using a JA-12 rotor (Beckman Coulter Avanti J-26 XPI centrifuge). The supernatant

was discarded, and pellets were collected and frozen at -80˚C.

2.1.2 Protein Purification

Frozen pellets were thawed on ice and each one was resuspended in 10 mL of loading

buffer (20 mM potassium phosphate, 0.3 M potassium chloride, 10 mM imidazole; pH 7.4)

containing 100 µL of 0.1 M phenylmethylsulfonyl fluoride (PMSF, a serine protease inhibitor),

and 100 µL of 0.1 M Tris(2-carboxyethyl)phosphine (TCEP, a reducing agent). The resulting cell

suspension was vortexed until a homogeneous suspension was achieved before being placed on

ice again. Resuspended cells were pooled in Falcon tubes, not exceeding a volume of 25 mL per

50 mL tube. While keeping them on ice, the cells were then lysed using a sonicator (Fisher

Scientific, Sonic Dismembrator, Model 100) set to a 70% intensity for 30 seconds at a time,

repeated 5 times per resuspended cell solution. The resulting lysate was centrifugated at 9,000 g

(7,470 rpm) and 4˚C for 20 minutes, using a JA-12 rotor (Beckman Coulter Avanti J-26 XPI

centrifuge) to remove cellular debris. Pellets were discarded and the supernatant was kept on ice.

Both gFlHb and Hmp were purified in the same manner by taking advantage of the

hexahistidine tag on their N-terminus. First, a 2 mL column of NiNTA Fast Flow resin (nickel

coupled to nitrilotriacetic acid) (Thermo-Fisher/Pierce; Ottawa, ON) was equilibrated with 2 mL

of loading buffer. The supernatant from the cell lysate was then loaded onto the column by

gravity flow, after which 2 mL of loading buffer was loaded onto the column. Following loading,

the column was washed with 10 mL of wash buffer (20 mM potassium phosphate, 0.3 M

potassium chloride, 25 mM imidazole, pH 7.4). The enzyme was then eluted by adding 1-2 mL

of elution buffer (20 mM potassium phosphate, 0.3 M potassium chloride, 400 mM imidazole;

pH 7.4) to release it from the column. When the resin approached saturation, a second column was used and treated in the same way.

Eluted enzyme solutions were concentrated by using an Amicon ultrafiltration unit with a 30 kDa molecular weight cutoff. Protein samples were loaded onto the ultrafiltration membranes and centrifuged at 5,000 g (5,568 rpm) and 4˚C for 20 minutes using a JA-12 rotor (Beckman Coulter Avanti J-26 XPI centrifuge). Any residual imidazole from the elution buffer was removed by size exclusion chromatography on a Superdex 200 column (10/300 GL) (Cytiva Life Sciences), connected to a fast protein liquid chromatography (FPLC) system (Pharmacia Biotech) using 100 mM potassium phosphate buffer, pH 7.4. Eluent was collected using a fraction collector and the fractions that had the strongest reddish color were pooled for subsequent storage. The volume was then recorded, and an equal volume of 100% glycerol was added to the solution to bring the glycerol concentration to 50% before measuring the concentration of the enzyme and storing it at -20˚C. The concentration of gFlHb/Hmp was measured in quartz cuvettes on a UV-vis spectrophotometer (Shimadzu, UV-1900i) at 403/405 nm, using an extinction coefficient of 139.7 mM^{-1}cm^{-1}. UV-visible spectra (250-800 nm) of purified proteins were also recorded. Purified flavohemoglobins were analyzed by SDS-PAGE (sodium dodecyl sulfate-polyacrylamide gel electrophoresis) using 10% gels on a Bio-Rad minigel system, run at a voltage of 150 v and stained with Coomassie Blue Dye.

2.2 Nitrite Detection Assays

2.2.1 The Griess Assay

The Griess assay for nitrite detection was performed in a 96-well microtiter plate. Each plate was used to screen for one FlHb inhibitor at a time. Ten different concentrations of each inhibitor were tested on the same plate for both gFlHb and Hmp, excluding the uninhibited

reactions for each enzyme, where the uninhibited NOD activity for each enzyme was used as a baseline. Tests were done with multiple replicates, consisting of 3-6 wells (4 for standards) with the same conditions for each treatment. A group of sodium nitrite standards (5) with known concentrations was used in order to create a trendline that would allow a linear regression to calculate nitrite concentrations in each sample to be made. The last treatment in each plate consisted of the NO donor in the absence of FlHb to assess the maximum possible concentration of nitrite obtained by the uncatalyzed oxidation of NO; this treatment served as a positive control.

The plate assay was performed on a FLUOstar Omega plate reader (BMG Labtech) and consisted of the addition of 5 different solutions to the plate (Table 3), for a total reaction volume of 100 µL prior to the addition of the Griess reagents. All reagents were mixed in Falcon tubes by pipetting up and down the contents before adding them to multichannel reservoirs that would facilitate the use of a multichannel micropipette for the microplate. The assays started with the addition of 45 µL of enzyme in Bis-Tris buffer (100 mM, pH 6.5) for an in-assay enzyme concentration of 100 nM for both gFlHb and Hmp as well as 1 µM FAD, except for the positive control where the whole of the volume was buffer. FAD was prepared from a 40 mM stock concentration that was diluted to 4 mM and stored at -20˚C. The concentration of FAD was checked by measuring the absorbance at 450 nm and using an extinction coefficient of 11.3 mM^{-1}cm^{-1}. After the addition of the enzyme, the plate was placed in the plate reader and the incubator feature was set to 37˚C. An incubation of 5 minutes is required prior to the addition of the ligand.

The second addition was the inhibitor to be tested; a total volume of 5 µL was added to each well, with varying inhibitor concentrations prepared in either Bis-Tris buffer (100 mM, pH 6.5) or the organic solvent dimethyl sulfoxide (DMSO) for ligands that were insoluble in water.

The standards, the blanks, and the positive control had no inhibitor added to them but instead the same volume (5 µL) of either buffer or DMSO. After the addition of the inhibitor or the solvent the shaker feature of the plate reader was turned on for 30 seconds at 300 rpm and the plate was incubated for 5 minutes prior to the addition of the NO donor or the nitrite standards.

Table 3: *Griess colorimetric assay plate procedure. List and order of addition of reagents.*

Order of addition	Reagent(s) and final concentrations	Volume (µL)
1[1]	**FlHb** (100 nM), **FAD** (1µM)	45
2[2]	**Inhibitor** (variable concentrations)	5
3[3]	**PROLI NONOate** (25 µM), **NADH** (100 µM)	40
4[1]	**LDH** (~0.3 U), **Pyruvate** (1 mM)	10
5	**Griess Reagents**	100

[1]*Prepared in 100 mM Bis-Tris (pH 6.5).* [2]*Prepared in 100% DMSO or 100 mM Bis-Tris (pH 6.5) for water-soluble ligands.* [3]*Prepared in 10 mM NaOH.*

The third solution to be added was the NO donor with the NADH cofactor. NADH was made fresh daily to a 10 mM stock concentration; the concentration of NADH was checked using the extinction coefficient 6.22 $mM^{-1}cm^{-1}$ for the absorbance value recorded at 340 nm. PROLI NONOate (10 mg) was dissolved in 4.566 mL of 10 mM NaOH and divided into aliquots that were stored at -80˚C. Each day, the concentration of PROLI NONOate for the aliquot to be used was checked at 252 nm, using an extinction coefficient of 8.40 $mM^{-1}cm^{-1}$. A total of 40 µL of NADH and PROLI NONOate (NO donor), prepared in NaOH buffer (10 mM) was added to each well for an in-assay concentration of 25 µM PROLI NONOate and 100 µM NADH. The addition of these substrates marks the beginning of the NOD reaction catalyzed by FlHbs. The plate was shaken at 300 rpm for 30 seconds and incubated for 10 minutes at 37˚C. To end the NOD reaction, 10 µL of lactate dehydrogenase (LDH) and pyruvate were added for an in-assay concentration of 0.3 U of LDH and 1 mM pyruvate. LDH was purified by the students in

CHEM3310 in the fall semester of the 2023-2024 academic year. Pyruvate was made by dissolving sodium pyruvate in 100 mM Bis-Tris (pH 6.5) to a concentration of 10 mM and stored at -20˚C. The addition of LDH and pyruvate consumes any remaining NADH that was not oxidized by gFlHb or Hmp, marking the end of the NOD reaction. This is an important step as NAD+, the oxidized product of NADH, does not interfere with the Griess assay (*vide infra*). The plate was shaken at 300 rpm for 30 seconds and incubated for 7 minutes at 37˚C.

In addition to these samples, the plate included five nitrite standards (0, 10, 20, 30, 40, and 50 µM). These wells were treated in an identical manner as described above. The only exception was that nitrite standards prepared in 10 mM NaOH replaced the PROLI NONOate and NADH solutions.

Lastly, the Griess reagents were added to each well of the plate to detect any nitrite present in the samples. The reagents required for the Griess reaction were labeled "Griess Reagent A" (sulfanilamide) and "Griess Reagent B" (NED). Griess Reagent A was made by diluting phosphoric acid from 85.6% to 4.25% and adding sulfanilamide to a concentration of 1%. Griess Reagent B was made by dissolving 1 g of *N*-(1-naphthyl)ethylenediamine dihydrochloride in 1 L of Millipore-grade water for a NED concentration of 0.1%. Griess Reagents A and B were stored in brown plastic bottles to protect them from light and were stored at 4˚C. Equal volumes of the Griess reagents were mixed in a reservoir using a serological pipette by pipetting up and down. 100 µL of the combined Griess reagents were added to each well. The plate was shaken at 300 rpm for 30 seconds and then the absorbance values for each well were measured at 550 nm. The absorbances of the six standards were used to create a standard curve that allowed for a linear regression to be made and measure the concentration of nitrite in each well.

2.2.2 DAN Fluorescence Assay

The fluorescence assay for nitrite detection was performed on the FLUOstar Omega plate reader (BMG Labtech) and used microplates that are specific for fluorescent measurements. The DAN assay encompasses the addition of six different solutions (Table 4) for a total reaction volume of 100 µL prior to the addition of DAN and NaOH. All reagents were mixed in Falcon tubes by pipetting up and down the contents before adding them to the multichannel reservoirs.

The first addition consisted of 45 µL of enzyme in Bis-Tris buffer (100 mM, pH 6.5) for an in-assay enzyme concentration of 30 nM for both gFlHb and Hmp as well as 1 µM FAD, except for the positive control where the whole of the volume was buffer. FAD was made by making a 40 mM stock concentration that was diluted to 4 mM and stored at -20˚C. The concentration of FAD was checked by measuring the absorbance at 450 nm and using an extinction coefficient of 11.3 mM^{-1}cm^{-1}. After the addition of the enzyme, the plate was placed in the plate reader and the incubator feature was set to 37˚C. An incubation of 5 minutes was used prior to the addition of the inhibitor. Next, inhibitor in a total volume of 5 µL was added to each well, with varying inhibitor concentrations prepared in either Bis-Tris buffer (100 mM, pH 6.5) or DMSO for inhibitors that were insoluble in water. The standards, the blanks, and the positive control had no inhibitor added to them but instead the same volume (5 µL) of either buffer or DMSO. After the addition of the inhibitor or the solvent control, the shaker feature of the plate reader was turned on for 30 seconds at 300 rpm and the plate was incubated for 5 minutes prior to the addition of the NO donor or the nitrite standards.

Table 4: *DAN fluorescent assay plate procedure. List and order of addition of reagents.*

Order of addition	Reagent(s) and final concentrations	Volume (µL)
1[1]	**FlHb** (30 nM), **FAD** (1µM)	45
2[2]	**Inhibitor** (variable concentrations)	5
3[3]	**PROLI NONOate** (3 µM), **NADH** (100 µM)	40
4[1]	**LDH** (~0.3 U), **Pyruvate** (1 mM)	10
5	0.05 mg/mL **DAN**	10
6	2.8 M **NaOH**	5

[1]Prepared in 100 mM Bis-Tris (pH 6.5). [2]Prepared in 100% DMSO or 100 mM Bis-Tris (pH 6.5) for water-soluble ligands. [3]Prepared in 10 mM NaOH.

NADH was made fresh daily to a 10 mM stock concentration, the concentration of NADH was checked using the extinction coefficient 6220 $M^{-1}cm^{-1}$ for the absorbance value recorded at 340 nm. PROLI NONOate was dissolved (10 mg) in 4.566 mL of 10 mM NaOH buffer and divided into aliquots that were stored at -80˚C. Each day, the concentration of PROLI NONOate for the aliquot to be used was checked at 252 nm, using an extinction coefficient of 8400 $M^{-1}cm^{-1}$. A total of 40 µL of NADH and PROLI NONOate dissolved in NaOH buffer (10 mM) was added to each well for an in-assay concentration of 3 µM PROLI NONOate and 100 µM NADH. There were 5 standards used for this assay with varying sodium nitrite concentrations (0, 1, 2, 3, 4, and 5 µM) and instead of PROLI NONOate and NADH, sodium nitrite diluted with NaOH (10 mM) was added to these wells, marking the beginning of the NOD reaction catalyzed by FlHbs. To end the NOD reaction, 10 µL of lactate dehydrogenase (LDH) and pyruvate were added for an in-assay concentration of 0.3 U of LDH and 1 mM pyruvate. LDH was purified by the students in CHEM3310 in the fall semester of the 2023-2024 academic year. Pyruvate was made by dissolving sodium pyruvate in 100 mM Bis-Tris (pH 6.5) to a

concentration of 10 mM and stored at -20˚C. The addition of LDH and pyruvate used up any remaining NADH that was not oxidized by gFlHb or Hmp, marking the end of the NOD reaction. This is an important step as NAD+, the oxidized product of NADH, does not interfere with the fluorescence assay (*vide infra*). The plate was shaken at 300 rpm for 30 seconds and incubated for 7 minutes at 37˚C.

Lastly, DAN and NaOH were added to the plate. DAN (TCI America; Portland, OR) was prepared in DMSO to a concentration of 2.5 mg/mL that was aliquoted in 1 mL vials and stored at -80˚C protected from light, as it is sensitive to it. A working solution of 0.05 mg/mL DAN in 0.62 M HCl was prepared freshly each day by adding 20 µL of the DAN stock to 360 µL of millipore water and 620 µL of 1 M HCl. After the incubation period that followed the addition of the LDH/pyruvate system, 10 µL of the DAN stock was added to each well. The plate was then shaken at 300 rpm for 30 seconds and incubated at 37˚C for 10 minutes. Next, 5 µL of 2.8 M NaOH was added to each well to quench the reaction, and the plate was shaken at 300 rpm for 30 seconds before measuring the fluorescent intensity of the wells. To measure the fluorescent intensity, the gain was set to 90% for the whole plate, the excitation wavelength was set to 360 nm, and the emission wavelength was set to 430 nm. After that, the plate was read, and the measurements obtained from the reading were given in terms of relative fluorescence units (RFU). The RFU values of the 6 standards were used to create a standard curve that allowed for a linear regression to be made and measure the concentration of nitrite in each well.

3. RESULTS AND DISCUSSION

3.1 Protein Expression

Proteins were judged pure by SDS-PAGE and the analysis of their spectra. The proteins

used in this study were deemed to be at least 95% pure, as seen in Figure 8, given the lack of

other major bands on the stained gel, indicating the successful isolation of the proteins of

interest. Both proteins can be seen where they are expected on the gel, given their molecular

weights (52 kDa for gFlHb and 44 kDa for Hmp). The absence of any other major bands on the

gel besides those of the proteins of interest indicates that the proteins were successfully purified.

The spectra of Hmp and gFlHb, Figures 9 and 10 respectively, are consistent with the spectra that

have been previously reported for these enzymes in our lab.
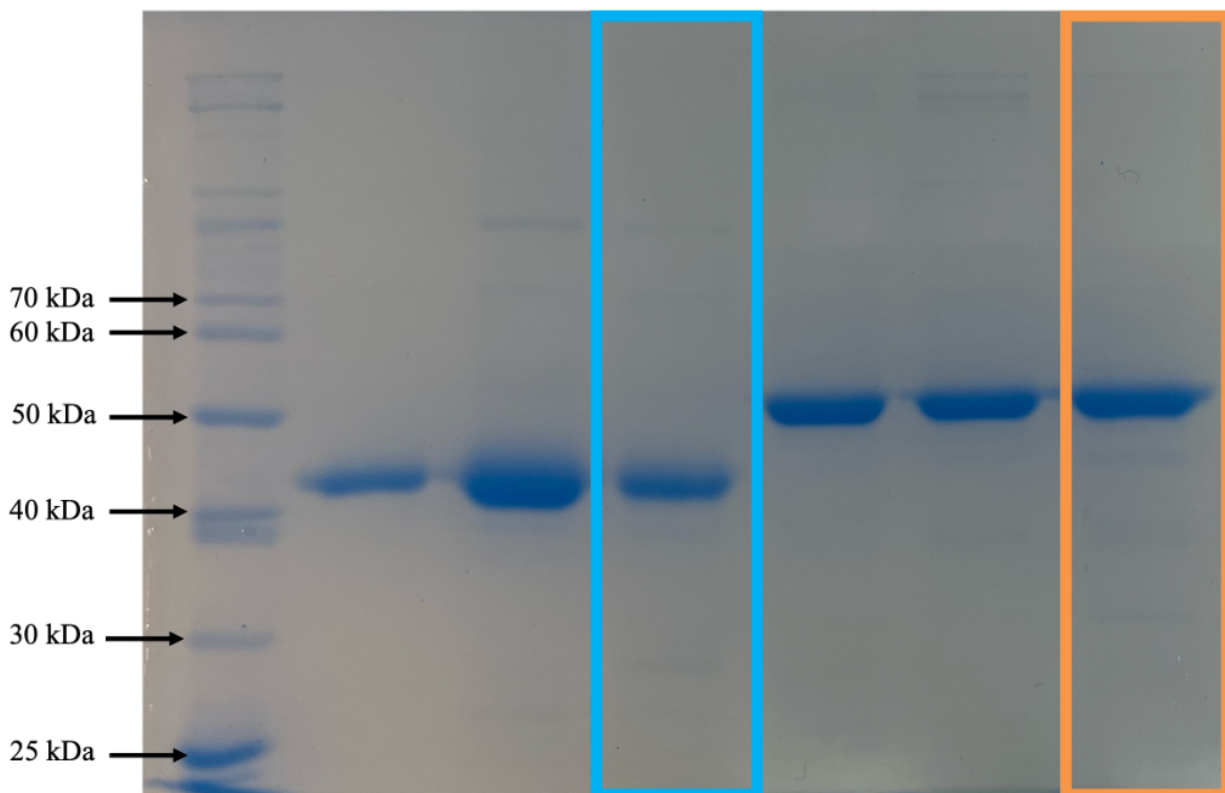
Figure 8: *SDS-PAGE results for Hmp (highlighted in blue) and gFlHb (highlighted in orange) with Coomassie Blue dye and an unstained protein ladder in the first lane from the left (p7717S New England Biolabs).*
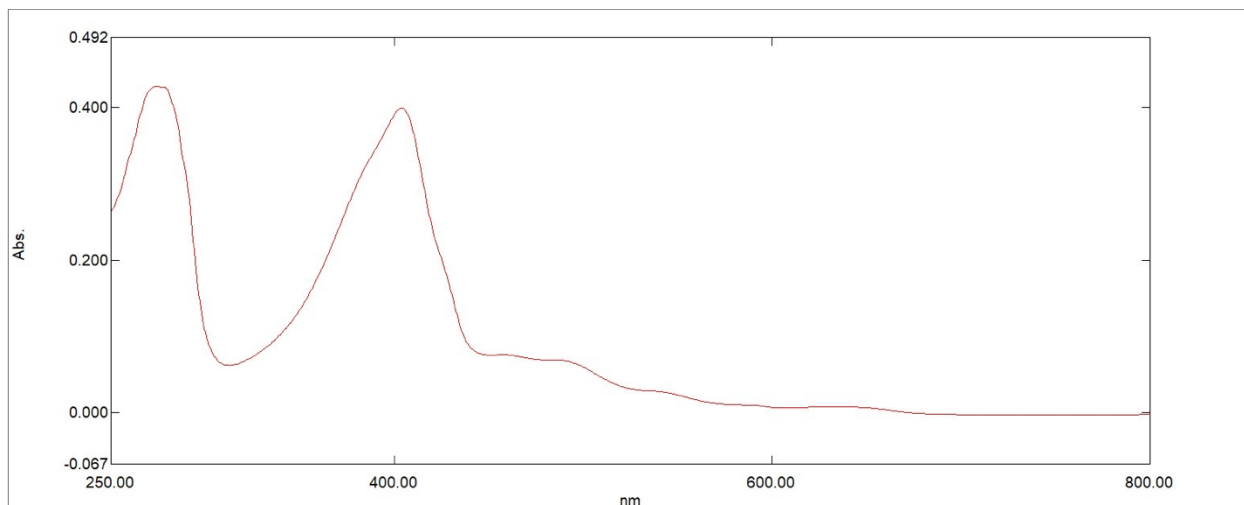
Figure 9: UV-visible spectrum of Hmp.
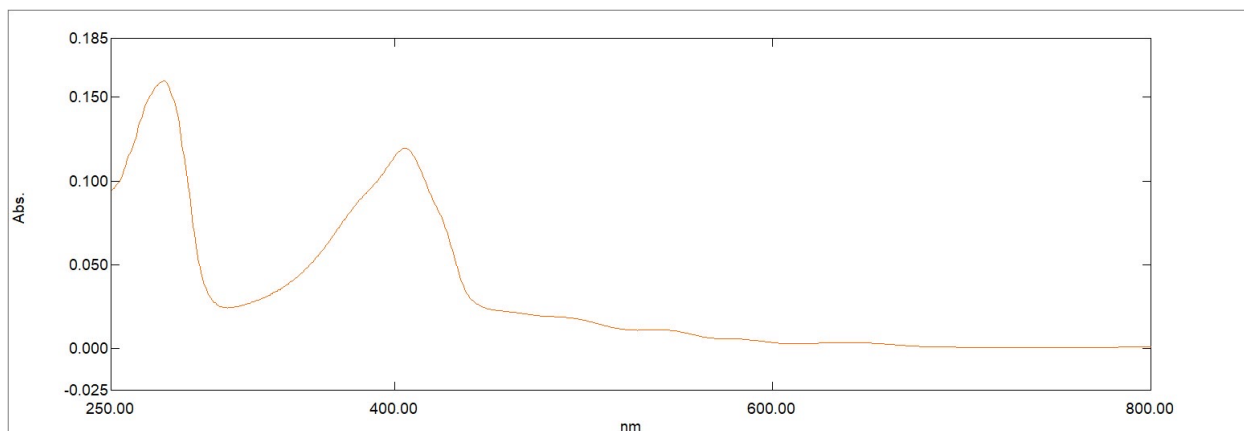
Figure 10: UV-visible spectrum of gFlHb.

3.2 Griess Assay Optimization

3.2.1 DMSO Interference

The optimization of the Griess assay required examining different variables that may interfere with the Griess reaction, which could skew the results that were to be obtained from the assay. As previously mentioned, FlHb inhibitors that were not water soluble were dissolved in the organic solvent DMSO. The first step was to assess whether this solvent had any effect on the Griess reaction. Figure 11 shows the absorbance readings obtained at 550 nm of a Griess reaction

where each set of data points corresponded to known nitrite concentrations in order to see whether DMSO had any effect on the measurements.
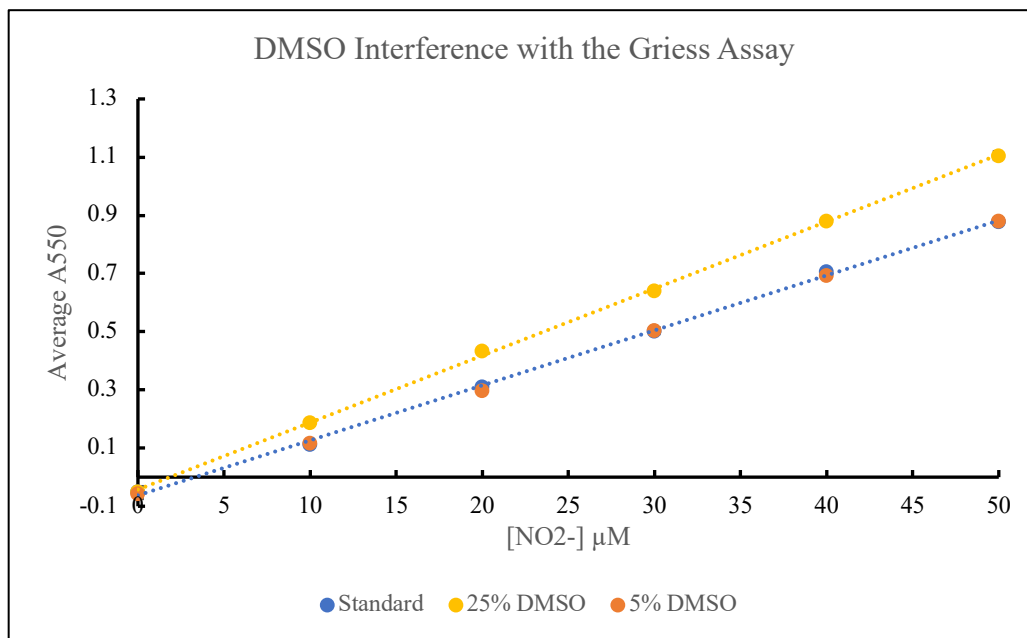
Figure 11: *Absorbance measurements at 550 nm of a group of standards with known nitrite concentrations and varying concentrations of the organic solvent DMSO, including standard error bars. Each data point represents the mean value for n=4 wells.*

Based on Figure 11, DMSO increases the absorbance measurements that are obtained from the Griess assay. The initial DMSO concentration that was tested was 25%, which corresponds to 25 µL of 100% DMSO used to dissolve an inhibitor. This volume corresponds to the volume that was initially used to deliver the drug into the solution. This concentration of DMSO in the solution has a significant effect on the Griess assay.

DMSO has the potential to interfere with the Griess assay via the aerobic oxidative coupling of the solvent which leads to the conversion of NED and sulfanilamide into the azo-product that is measured (Lin et al., 2016). A lower concentration of DMSO was then tested to minimize the effects of DMSO on the assay. 5% DMSO corresponds to the lowest volume that could be delivered to a well by using our multichannel micropipette, which has a range of 5-50

µL (BRANDTECH Scientific) and is the limiting factor for the volume that could be used. The absorbance readings obtained from the samples containing a concentration of 5% DMSO align with those of the standards that had no DMSO in the solutions, suggesting that 5% was the optimal concentration to be used for drug deliverance in order to decrease assay interference. To ensure no further effects of this solvent on the assay, 5% DMSO was to be added to all samples, including blanks, standards, and controls.

3.2.2 NADH Interference

NADH, the electron donor for the NOD reaction of FlHbs, is a known inhibitor of the Griess reaction as noted by Bryan & Grisham (2007), while the oxidized cofactor NAD^+ does not interfere with this reaction. NADH has the potential to interfere with the Griess reaction via the loss of nitrite through its reduction by NADH at the low pH present in the reaction or by the loss of a diazonium ion through its reduction by NADH prior to the reaction with NED (Moody & Shaw, 2006). Figure 12 shows the extent of the interference with the Griess reaction caused by NADH present in the sample. Here, A_{550} measurements of a set of standards with known nitrite concentrations are presented in the presence or absence of 100 µM NADH.

The set of standards containing NADH yielded ~30% lower absorbance measurements than the set that had no NADH. These results showed that the NADH cofactor, which is the ultimate electron donor for FlHbs has detrimental effects on the absorbance measurements and can skew the results that are obtained from the Griess assay. In the absence of NADH the true absorbance values would be higher than the ones obtained, indicating that all the NADH must be oxidized to NAD^+ prior to the addition of the Griess reagents in order to obtain accurate measurements.
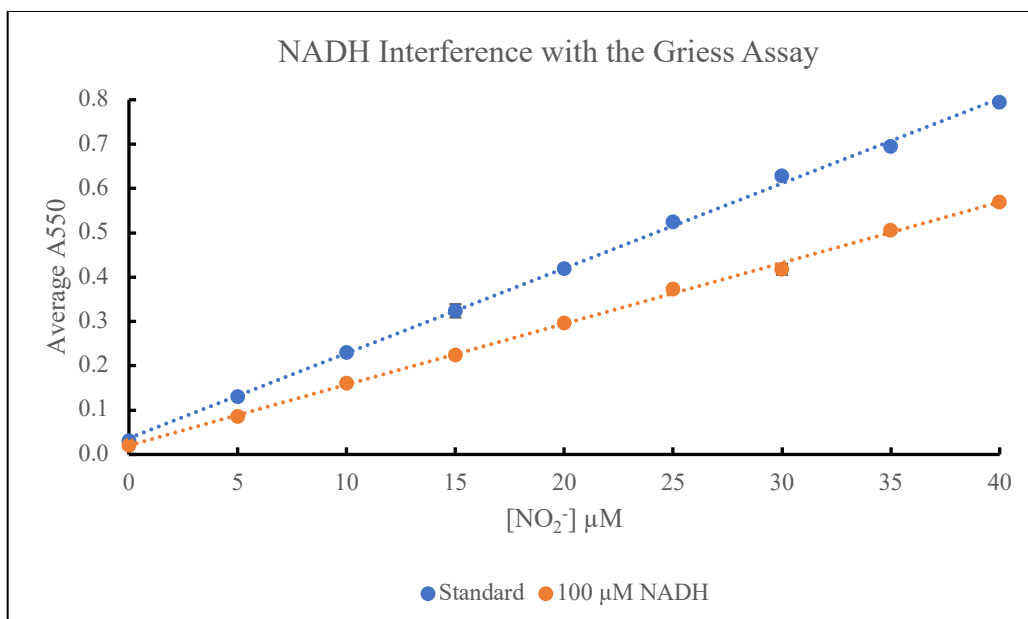
Figure 12: *Absorbance measurements at 550 nm of a group of standards with known nitrite concentrations vs. the same concentrations of nitrite in the presence of 100 μM NADH, including standard error bars. Each data point represents the mean value for n=8 wells.*
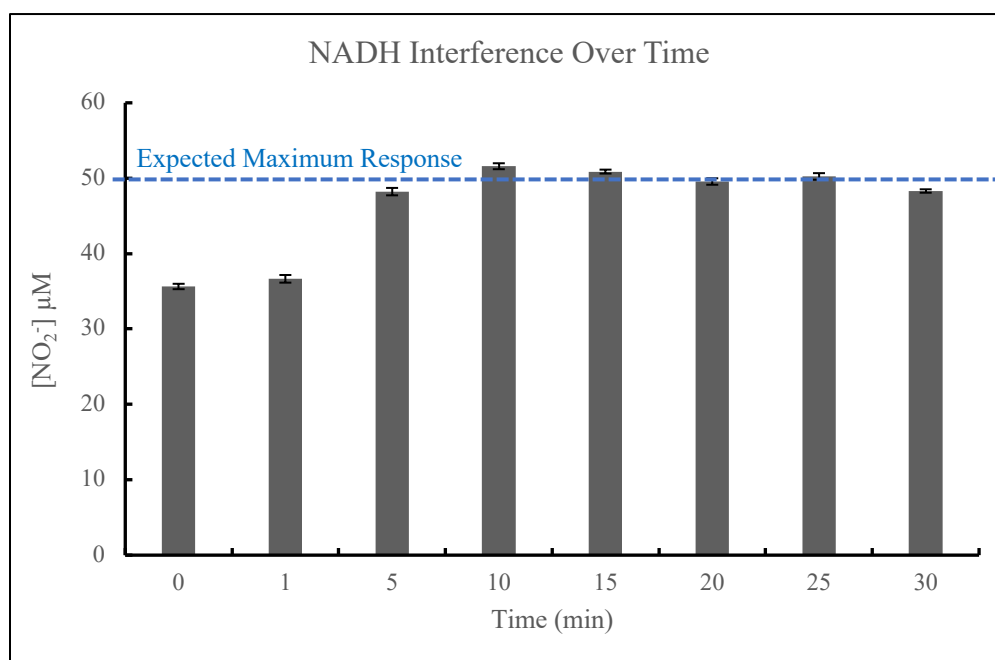
Figure 13*: Griess assay with gFlHb (100 μM) to assess how long it would take to consume 100 μM NADH. A linear regression was made from a standard curve to determine nitrite values, including standard error bars. Each data point represents the mean value for n=8 wells.*

It was initially thought that FlHbs could efficiently clear all the NADH present in the solution owing to their ability to oxidize NADH in the absence of NO, as supported by the results seen in Figure 13. Figure 13 shows the results of a linear regression from an experiment that varied the time of addition of the Griess reaction to a solution containing gFlHb and 50 µM nitrite. In this set of experiments, it took approximately 10 minutes for the NADH-oxidase activity of the enzyme to oxidize all the NADH that was present in the solution (100 µM). However, this failed to account for the effects of inhibitors on NADH-oxidase activity in addition to its NOD activity. Indeed, Helmick et al. (2005), found that drugs such as miconazole interfere with the NADH-mediated reduction of heme, indicating that NADH would not be completely oxidized prior to the addition of the Griess reagents and the completion of the Griess reaction.
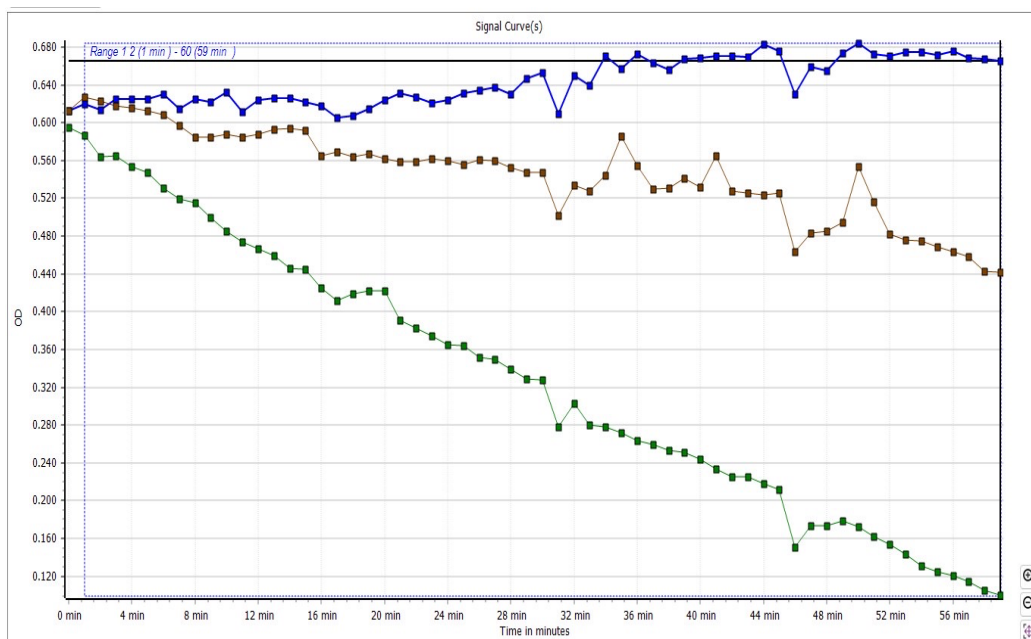
Figure 14: *Kinetic trace measuring NADH-oxidase activity of 10 µM Hmp. The top blue line corresponds to 100 µM NADH. The bottom green line corresponds to the NADH-oxidase activity of 10 µM Hmp. The middle brown line corresponds to the NADH-oxidase activity of 10 µM Hmp in the presence of 10 µM miconazole. n=1 well.*

The ability of NOD activity inhibitors to impede NADH oxidation was confirmed in an experiment in which miconazole was present in the assay (Figure 14). It is evident that in the presence of a known FlHb inhibitor, the NAHD-oxidase activity of the FlHbs is much lower. In the presence of NOD inhibitors, the inherent NADH-oxidase activity of FlHb cannot be relied on to completely oxidize this cofactor before the addition of the Griess reagents.
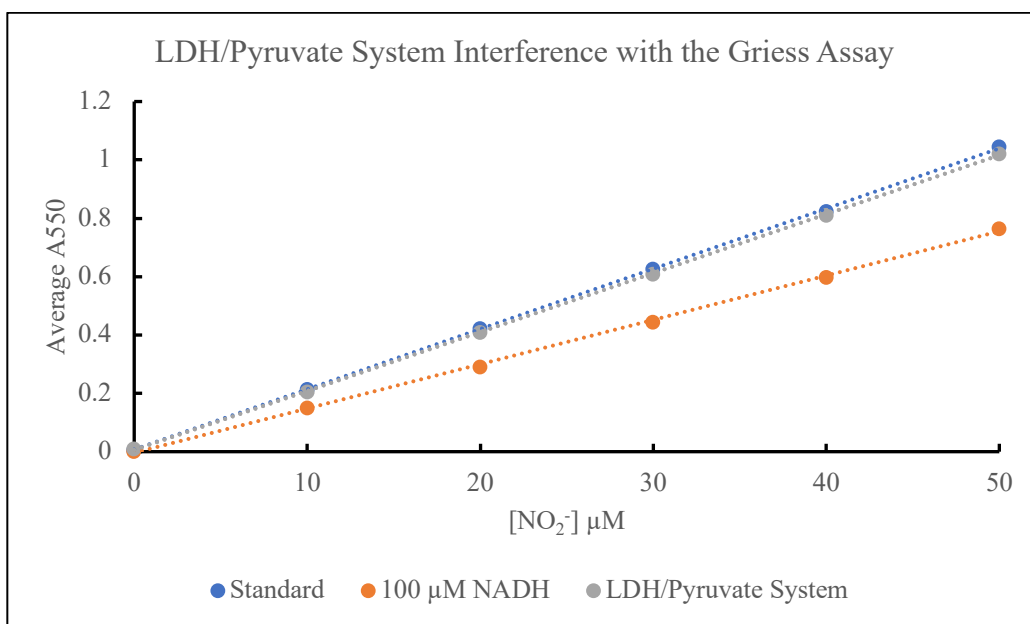
Figure 15: *Absorbance measurements at 550 nm of a set of standards with known nitrite concentrations (shown in blue), compared to the same standards with 100 µM NADH and the presence (shown in grey) or absence (shown in orange) of the LDH/Pyruvate system, including standard error bars. Each data point represents the mean value for n=3 wells.*

As NADH must be cleared from any solution that is to be measured via the Griess assay given its inhibitory nature, one possibility is to use a second enzyme-catalyzed reaction that oxidizes NADH, such as that catalyzed by the enzyme lactate dehydrogenase (LDH), as described by Grisham et al. (1996). LDH catalyzes the reversible conversion of pyruvate to lactate and the oxidation of NADH to NAD^+. The reaction is driven in the desired direction of NADH oxidation by the addition of excess pyruvate.

Figure 15 displays the results of an experiment that tested the ability of the LDH/Pyruvate system to oxidize unreacted NADH after a NOD inhibition reaction before the addition of the Griess reagents. In this figure, the extent of the interference of NADH with the Griess assay can be appreciated by the lower absorbance readings, as opposed to the oxidation of NADH seen with the LDH/Pyruvate system, which is almost identical to the values obtained from a group of standards that had no NADH present in the solution, indicating that the addition of LDH and pyruvate successfully oxidized NADH. It was then determined that any future experiments were to include excess pyruvate (1 mM) and LDH (0.3 U) to ensure that any NADH that had not been consumed was cleared from the solution prior to the addition of the Griess reagents. The addition of the LDH/Pyruvate system marks the end of the NOD reaction and is done with the sole intention of clearing the NADH, with the aim of preventing the inhibition of the Griess reagents.

3.2.3 Enzyme Concentration

The last variable that required optimization prior to beginning the testing of drugs with the Griess assay was the optimal concentration of FlHbs to be used. Initially, a 1 µM concentration of FlHb in the assay was used as that appeared to be the consensus reached by previous students in the Rafferty lab. However, this seemed wasteful of enzyme; typically, an enzyme preparation yielded about 10 mL of 10 to 25 µM purified enzyme. Therefore, determining what the optimal concentration of enzyme to be used would allow to use lower amounts of enzyme, which would minimize the expense and time spent on enzyme purification. Figure 16 shows the results of a linear regression that looks at the NOD activity of gFlHb in the presence and absence of imidazole. These results show that enzyme assay concentrations as low as 100 nM can be used in experiments to detect the inhibition of the NOD activity.
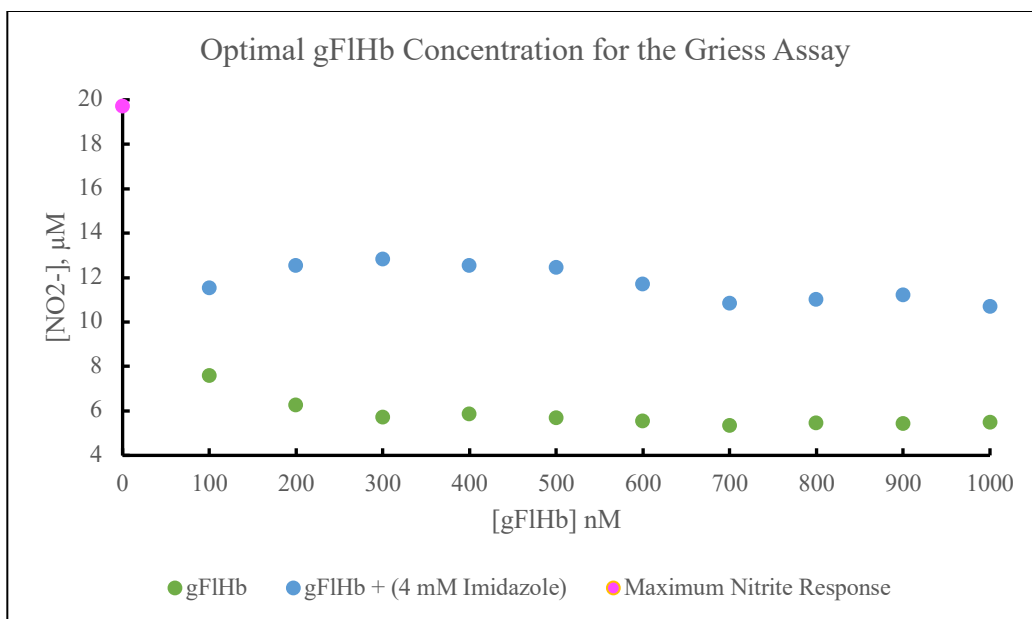
Figure 16: *Linear regression from the Griess assay that tested the NOD activity of different gFlHb concentrations in the presence or absence of an inhibitor in order to determine the optimal enzyme concentration to be used for experiments, including standard error bars. Each data point represents the mean value for n=3 wells.*

3.2.4 Griess Assay Remarks

The Griess assay was shown to be a rapid, non-expensive, and effective way to measure nitrite concentrations present in a solution. Nonetheless, optimizing the assay required looking at the different variables that could interfere with the Griess reaction and skew the results. Among these variables, DMSO proved to increase the value of absorbance measurements when used at an in-assay concentration of 25%. In order to decrease the extent to which DMSO affects the absorbance readings, the volume of DMSO that was used for the delivery of drugs was lowered to 5 µL, which translated to an in-assay concentration of DMSO of 5%. This concentration was shown to not alter the absorbance measurements in a significant manner, thus indicating that it was the optimal concentration of DMSO to be used.

Another variable that proved to interfere with the Griess assay was the use of NADH, a known Griess reaction inhibitor and a required cofactor for FlHbs, which lowered the absorbance

values recorded from the experiments by ~30%. FlHbs are effective in clearing NADH present in a solution. Nonetheless, in the presence of a FlHb inhibitor, NADH is not successfully cleared, and the use of a second-enzyme catalyzed reaction is required. The LDH/pyruvate system was proven to be effective in oxidizing all unreacted NADH to NAD^+, which does not interfere with the Griess reaction.

The last variable that was optimized was the concentration of enzyme to be used. This was done with the purpose of minimizing the expense and time spent on enzyme purification. It was determined that a concentration of 100 nM FlHb was the optimal concentration to be used for the Griess assay as it was the lowest concentration that was tested, which allowed detection of NOD activity inhibition.

3.3 Fluorescence Assay Optimization

3.3.1 DMSO Interference

The issues and solutions that arose while optimizing the Griess assay played a major role in the optimization of the fluorescence assay. The first step was to assess DMSO interference, given that the fluorescence assay is fifty to one hundred-fold more sensitive than the Griess assay (Misko et al., 1993). Figure 17 shows the results of an experiment that measured the effect of 5% DMSO on the fluorescence assay as this was the DMSO concentration that was optimal for the Griess assay and was also the lowest possible concentration, based on the settings of the multichannel micropipette. Fluorescence measurements yielded ~ 15% higher RFU values for the samples containing DMSO than those that had none. It is possible that DMSO causes a similar reaction as that seen with the Griess assay where DMSO causes the aerobic oxidative coupling of DAN molecules (Lin et al., 2016). It is also possible that DMSO changes the overall solution characteristics, by preventing interaction with water molecules and impacting

fluorescence readings (Markarian & Shahinyan, 2015). To account for the increase in the

sensitivity, DMSO was added to the same concentration for all samples, standards, blanks, and

controls.
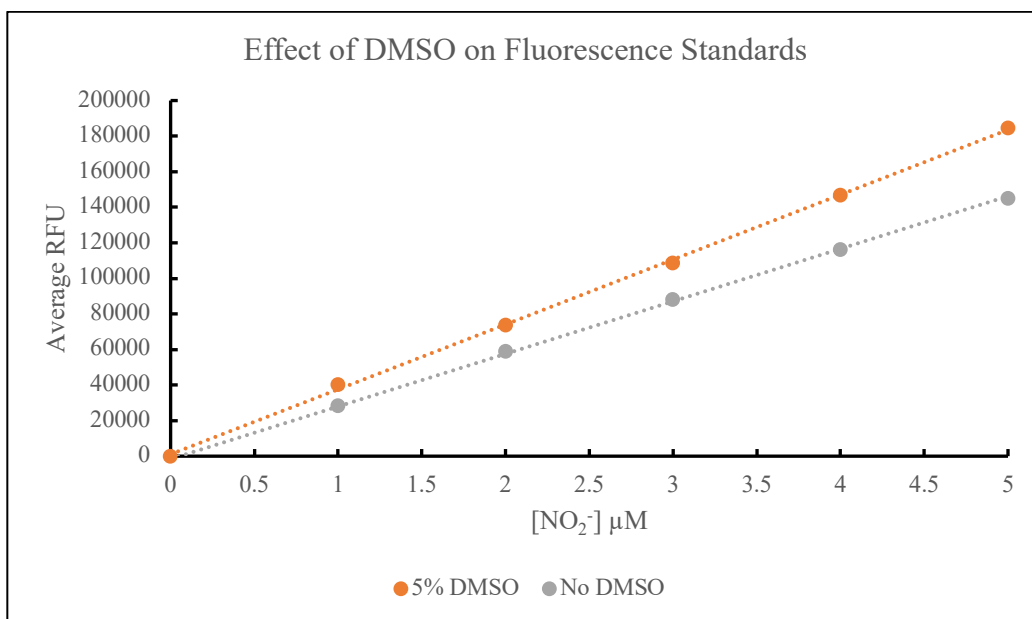
Figure 17: *Fluorescence measurements of a group of standards with known nitrite concentrations and a group of standards with the addition of 5% DMSO, including standard error bars. Each data point represents the mean value for n=4 wells.*

3.3.2 NADH Interference

The sensitive nature of the fluorescence assay proved to be highly susceptible to NADH

interference as evidenced by Figure 18. In this figure, two sets of standards were tested, one with

no NADH and one with 100 µM NADH. The fluorescent signal of samples that contained

NADH was ~ 70% lower than those with no NADH. Similarly to the Griess assay, NADH may

interfere with the fluorescence assay via the loss of nitrite through the reduction by NADH at the

low pH required for this reaction (Moody & Shaw, 2006). Previous experience with the Griess

assay played a vital role in the solution to this problem as it was known that inhibitors would

affect the NADH-oxidase activity of FlHbs resulting in leftover unreacted NADH in the sample.

The approach that was used to solve NADH interference was the same that was used for the

Griess assay, which was the implementation of the LDH/Pyruvate system.
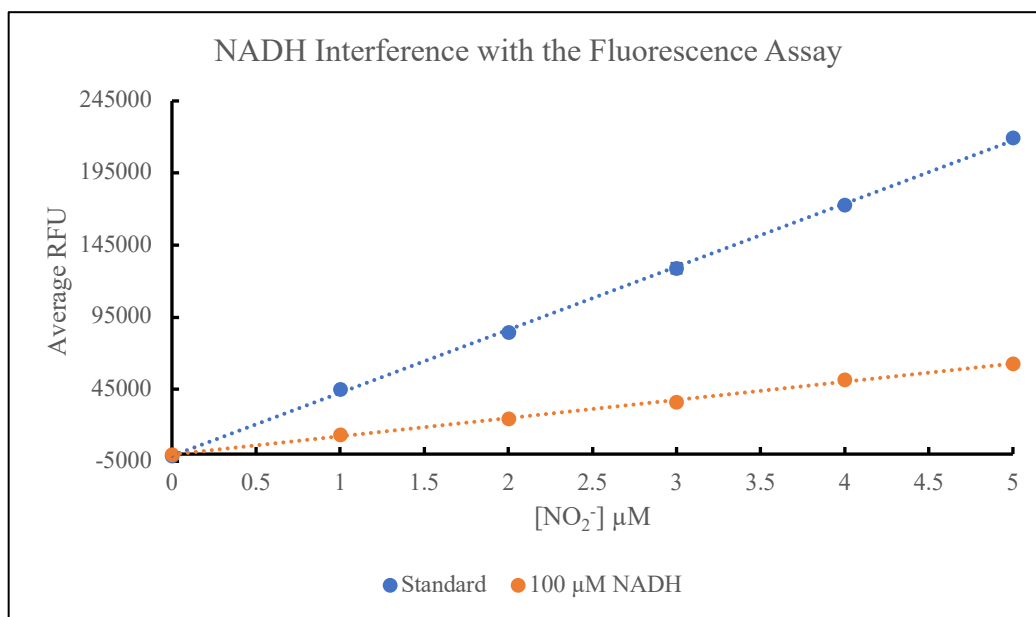
Figure 18: *Fluorescent measurements of a group of standards with known nitrite concentrations vs. the same concentrations of nitrite in the presence of 100 μM NADH, including standard error bars. Each data point represents the mean value for n=3 wells.*
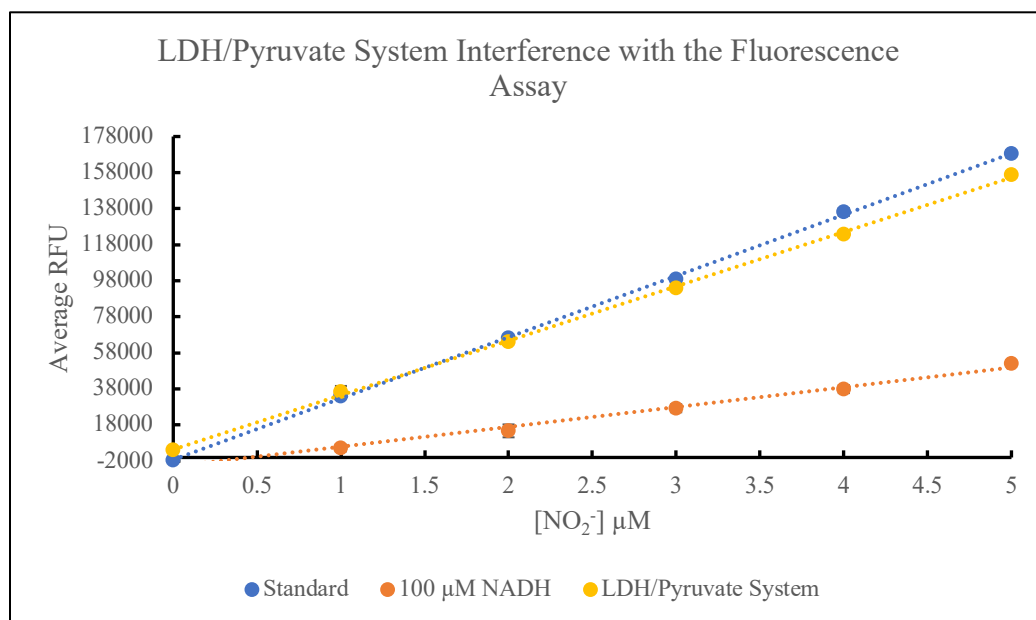
Figure 19: *Fluorescence measurements of a set of standards with known nitrite concentrations (shown in blue), compared to the same standards with 100 μM NADH and the presence (shown in yellow) or absence (shown in orange) of the LDH/Pyruvate system, including standard error bars. Each data point represents the mean value for n=3 wells.*

The effects of the LDH/Pyruvate system on the fluorescence assay are shown in Figure 19 and show how this system is effective in using up any remaining NADH. This experiment was performed under the same experimental conditions as the one that was performed with the Griess assay (Figure 15). Here, DAN and 2.8 M NaOH were added to the samples shown in Figure 19 instead of the Griess reagents. The concentrations of pyruvate, LDH, and NADH used for the fluorescence assay were the same ones used for the Griess assay, proving once again that the LDH/Pyruvate system is the most efficient method to oxidize NADH and obtain true fluorescent measurements.

3.3.3 Age of the DAN Stock Solution

Misko et al. (1993) highlighted that the age of the DAN stock solution being used had an effect on the intensity of the fluorescence of the sample. To assess how the age of the DAN stock solution affected fluorescent measurements, two different stocks of DAN were used. One stock solution was prepared in 2021, 2.5 years before these studies, while the other one was prepared freshly, the week before the experiment was performed.

This experiment consisted of two sets of standards of known nitrite concentrations and the addition of the different DAN stock solutions to each set of standards (Figure 20). The intensity of the fluorescent signal corresponding to the fresh DAN stock solution is much higher than the older DAN stock solution. Even though the magnitude of the response seems to follow the same linear trend, the intensity of the signal is stronger with the fresh DAN stocks, indicating that any experiments that were to be performed moving forward would require the use of fresh DAN stock solutions. Nonetheless, it is important to keep in mind that the literature suggests the use of DAN stocks prepared within six months of the intended date for all experimental procedures, despite not testing a solution that was exactly six months old in this study.
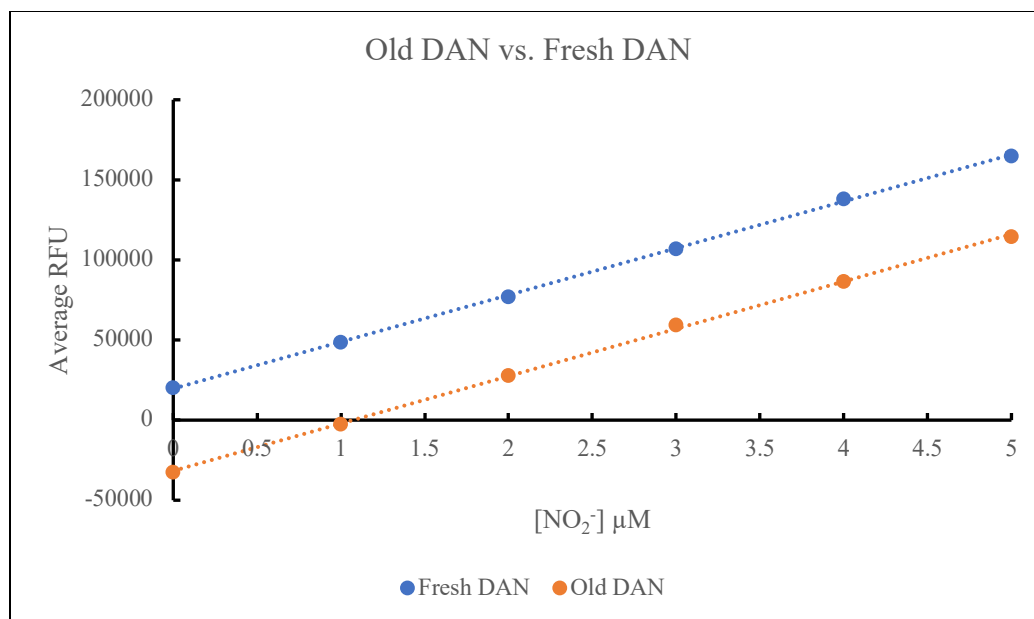
Figure 20: *Fluorescent measurements of a group of standards with known nitrite concentrations after the addition of DAN prepared at different times. In blue, DAN that was prepared within 6 months of use vs. 2 years, shown in orange, including standard error bars. Each data point represents the mean value for n=4 wells.*

3.3.4 Enzyme Concentration

Another variable that required optimization before beginning the testing of drugs with the fluorescence assay was the optimal concentration of FlHbs to be used. Since the fluorescence assay is much more sensitive than the Griess assay, the enzyme concentrations that were tested for the optimization were lower than the ones tested for the Griess assay (Figure 16) by a factor of 10. Figure 21 shows the results of a linear regression that looks at the NOD activity of gFlHb in the presence and absence of imidazole. The optimal concentration to be used for the fluorescence assay was determined to be 30 nM as shown in Figure 21. This selection was made because the uninhibited reaction of gFlHb showed the highest NOD activity at 30 nM while it showed the lowest NOD activity in the presence of 4 mM imidazole. This concentration was selected in place of 10 or 20 nM since it allowed for the use of a volume of enzyme that was easier to manage and handle. If the concentration of enzyme that was chosen was lower, the

volume of buffer needed to dilute it would have been too low for the reservoirs as well as the use of micropipettes that were able to handle much lower volumes than the ones being used. This choice was made as a matter of convenience.
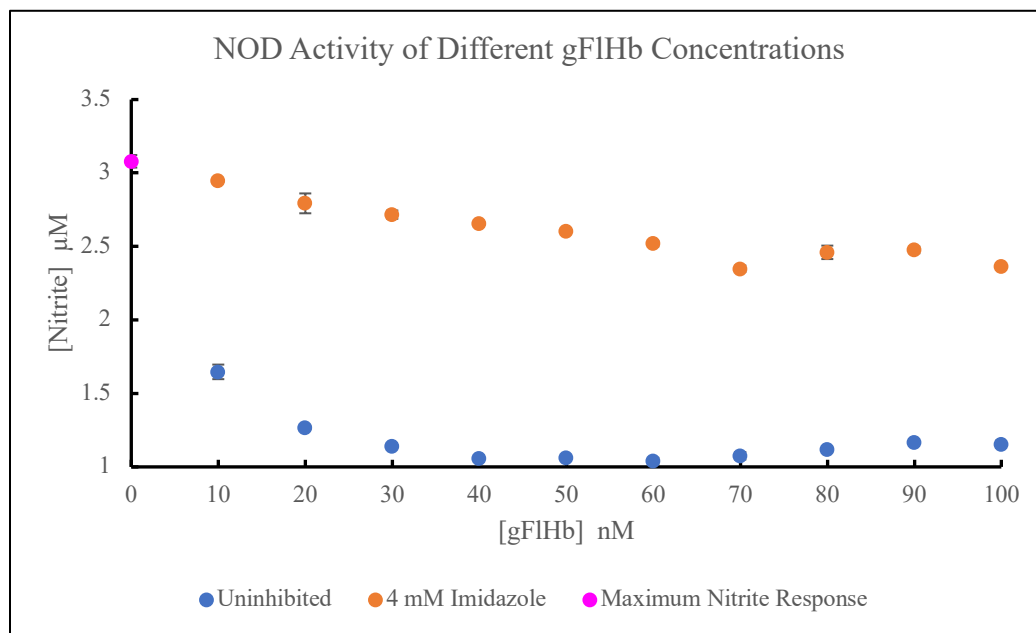
Figure 21: *Linear regression from the Fluorescence assay that tested the NOD activity of different gFlHb concentrations in the presence of an inhibitor in order to determine the optimal enzyme concentration to be used for experiments, including standard error bars. Each data point represents the mean value for n=3 wells.*

3.3.5 Fluorescence Assay Remarks

The fluorescence assay was proven to be a rapid and effective way to detect nitrite in a solution, though it is not as inexpensive as the Griess assay. The fluorescence assay was shown to display higher sensitivity than the Griess assay, allowing the detection of nitrite concentrations as low as 3 µM. The optimization of this assay was very similar to that of the Griess assay and, encompassed the assessment of the effect of DMSO and NADH on this assay, as well as the concentration of enzyme to be used in the experiments. The only different variable that was assessed for the fluorescence assay was the effect of the age of the DAN reagent on the fluorescent measurements.

DMSO affected the fluorescence assay in a similar way than it affected the Griess assay, though the extent of its interference is much greater, given the sensitive nature of this assay. Nonetheless, it was decided that the optimal concentration of DMSO to be used was 5%, as that was the lowest volume that could be delivered by our multichannel micropipette. NADH also affected the fluorescence assay to a much greater extent than it affected the Griess assay. Once again, the use of the LDH/pyruvate system proved to be effective in oxidizing any unreacted NADH and providing accurate fluorescent measurements. Similarly to the Griess assay, the concentration of enzyme to be used was determined in order to minimize the expense and time spent on enzyme purification. The optimal concentration of enzyme to be used was determined to be 30 nM.

The last variable that was studied for the required optimization of the fluorescent assay was the effect of the age of the DAN reagent. The literature suggested that the age of the DAN stock had an effect on the intensity of the fluorescence of the sample. This was supported by a much lower intensity of the recorded fluorescent values of the older DAN stock when compared to the fresher stock, thus indicating that any subsequent experiments require the use of fresh DAN stocks.

3.4 Imidazole-Based Ligands

The Griess assay and the fluorescence assay for nitrite detection were used to screen a group of six imidazole-based ligands (Table 1) as potential gFlHb inhibitors. These compounds were selected based on the ability of four of them to bind Hmp (miconazole, econazole, clotrimazole, and ketoconazole) as demonstrated by Helmick et al. (2005). Metronidazole was selected as it is a nitroimidazole-based molecule that is the preferred drug of choice for the treatment of giardiasis (Mørch & Hanevik, 2020). Lastly, imidazole was selected as it is the

structural basis for all the other ligands to be screened, and the fact it effectively binds to globins, including gFlHb (Nezamololama, M.Sc. Thesis, 2019). The concentrations of ligands that were tested were determined based on the inhibition constants (K_i values) determined by Helmick et al. (2005).
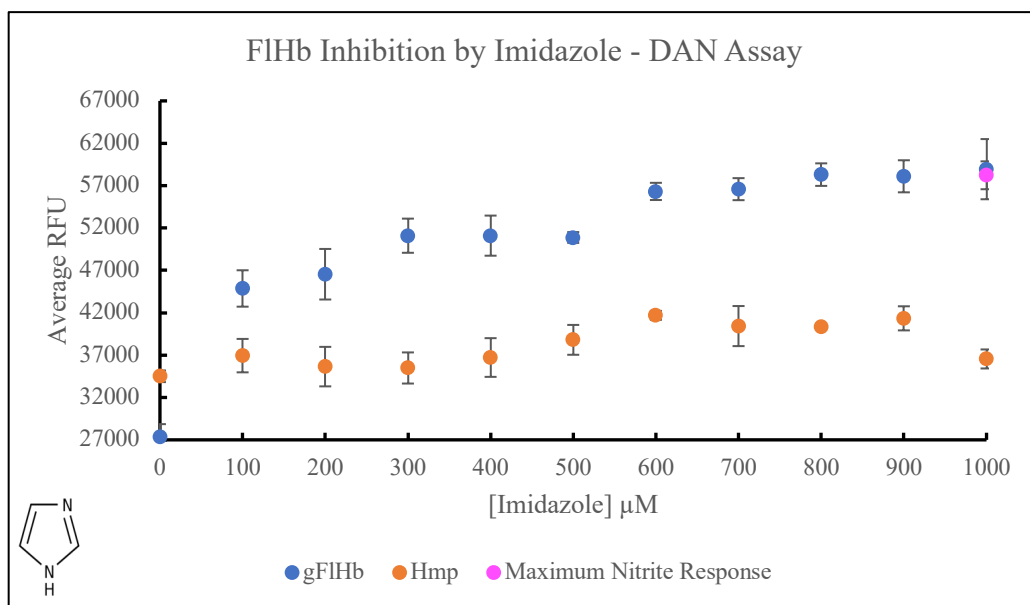
3.4.1 Imidazole

The first inhibitor that was tested was imidazole. Previous studies by members of the Rafferty laboratory had shown its ability to bind to gFlHb. This, and the fact that it is water-soluble and inexpensive (~ 35¢/g) are the reasons why it was the first inhibitor that was tested as well as the one that was used for the optimization of both assays. Figure 22 and Figure 23 depict the results of the optimized assays upon testing various concentrations of imidazole (0-1000 µM). These results represent how successful imidazole was in inhibiting the NOD activity of gFlHb and Hmp, with both figures exhibiting the same trends for both enzymes.
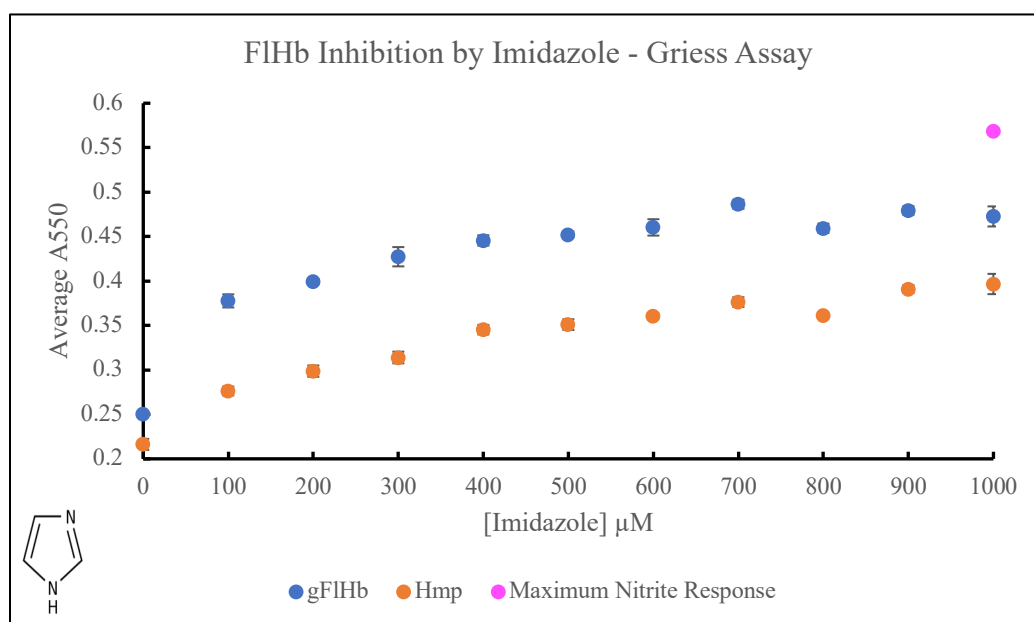
Figure 22: *Griess assay results assessing the NOD activity of FlHbs in the presence of imidazole. Blue denotes the accumulation of nitrite in the experiments with gFlHb, and orange with Hmp. The pink circle indicates the maximum response for the full conversion of NO to nitrite by uncatalyzed oxidation with no flavohemoglobin present. This figure includes standard error bars, and each data point represents the mean value for n=3 wells.*

Imidazole is the smallest one of the ligands used in this study at 68.08 g/mol and based on Figure 22 and Figure 23 it partially inhibits both flavohemoglobins. Nonetheless, it is a more effective inhibitor of gFlHb than Hmp, as supported by the higher absorbance and fluorescence measurements obtained from the gFlHb samples than those seen with Hmp, indicating higher concentrations of nitrite in the solution and a less effective NOD activity in the presence of imidazole. Imidazole is the ligand that caused the highest inhibition of gFlHb. However, it is important to note that the concentrations of imidazole required for the inhibition of gFlHb are high (200-1000 µM) and that if it were to be used therapeutically, the amount of imidazole that would need to be provided to a patient would be evidently higher than the required therapeutic dose. Furthermore, imidazole lacks specificity as a potential ligand to other heme proteins including globins, cytochrome P450 monooxygenases, nitric oxide synthases, and catalases. Nonetheless, imidazole has been useful in defining the assay conditions developed in this thesis.

Figure 23: *Fluorescence assay results assessing the NOD activity of FlHbs in the presence of imidazole. Blue denotes the accumulation of nitrite in the experiments with gFlHb, and orange with Hmp. The pink circle indicates the maximum response for the full conversion of NO to nitrite by uncatalyzed oxidation with no flavohemoglobin present. This figure includes standard error bars, and each data point represents the mean value for n=3 wells.*
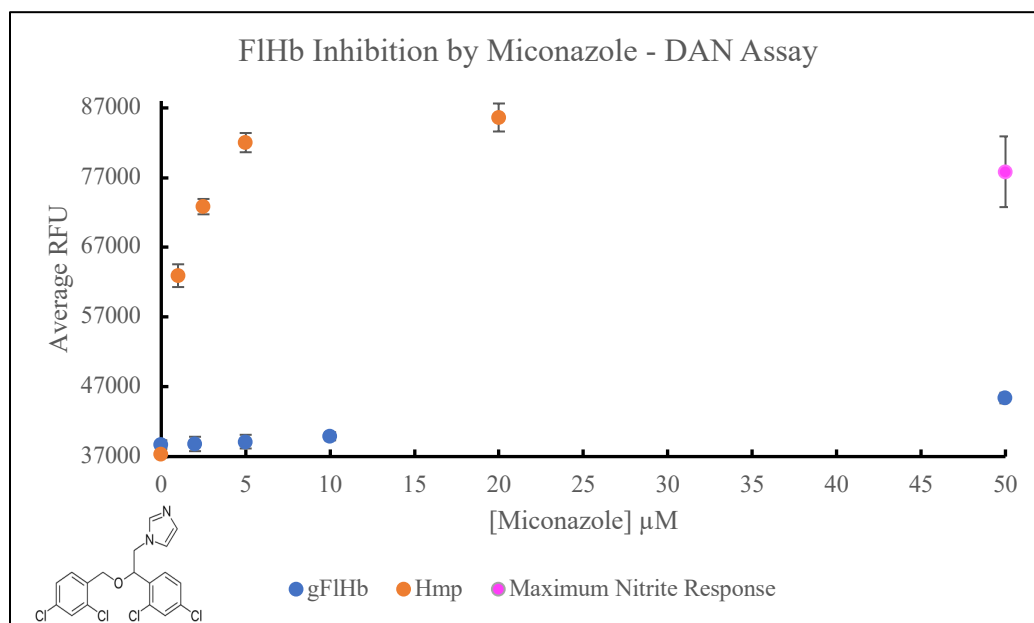
3.4.2 Miconazole

Miconazole was one of the largest compounds tested throughout this study, with a molar mass of 416.13 g/mol, and the best Hmp inhibitor, with a K_i of 80 nM, as determined by Helmick et al. (2005). Their results align with those obtained from this study as supported by the Griess (Figure 24) and fluorescence (Figure 25) assays. Figure 24 and Figure 25 show how miconazole almost causes the full inhibition of Hmp and how it barely causes any inhibition of gFlHb. This is supported by the low concentrations of miconazole required to inhibit Hmp to any extent as opposed to gFlHb.
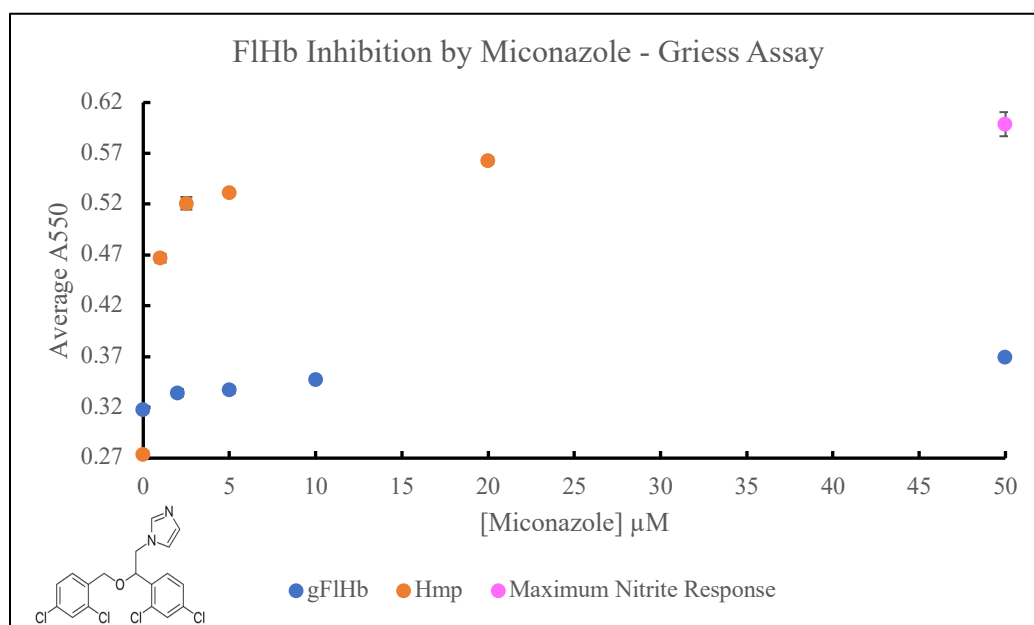
Figure 24: *Griess assay results assessing the NOD activity in the presence of miconazole. Blue denotes the accumulation of nitrite in the experiments with gFlHb, and orange with Hmp. The pink circle indicates the maximum response for the full conversion of NO to nitrite by uncatalyzed oxidation with no flavohemoglobin present. This figure includes standard error bars, and each data point represents the mean value for n=6 wells.*

Figure 24 and Figure 25 show how a concentration as low as 1 μM causes the partial inhibition of Hmp. The absorbance and fluorescence measurements of 1 μM miconazole for Hmp are higher than the ones obtained from the highest concentration of miconazole used for

gFlHb (50 µM) indicating that Hmp has a higher affinity for miconazole than gFlHb. Even after

using 50 µM miconazole the inhibition of gFlHb is extremely poor.

Figure 25: *Fluorescence assay results assessing the NOD activity of FlHbs in the presence of miconazole. Blue denotes the accumulation of nitrite in the experiments with gFlHb, and orange with Hmp. The pink circle indicates the maximum response for the full conversion of NO to nitrite by uncatalyzed oxidation with no flavohemoglobin present. This figure includes standard error bars, and each data point represents the mean value for n=6 wells.*

If Figure 24 shows the magnitude of the inhibition of Hmp in comparison to that of

gFlHb, this difference becomes more obvious in Figure 25, due to the more sensitive nature of

the fluorescence assay and its ability to detect low nitrite concentrations present in the solution.

Nonetheless, Figure 25 successfully exhibits similar levels of inhibition by miconazole for both

enzymes as seen with the Griess assay. These results differ from those seen with imidazole as not

only is Hmp more sensitive to miconazole than gFlHb, but the latter is also not inhibited as

much, even at high ligand concentrations.

3.4.3 Econazole

Figure 26 depicts the results of the Griess assay in the presence of various concentrations

of econazole, one of the three largest ligands tested throughout this study at 381.68 g/mol. Based

on its previously reported *Ki* value, econazole is the second best Hmp inhibitor after miconazole

with a K_i of 550 nM (Helmick et al., 2005). The results of the experiments conducted in this

study show that contrary to what was seen with miconazole, econazole only causes the partial

inhibition of Hmp.
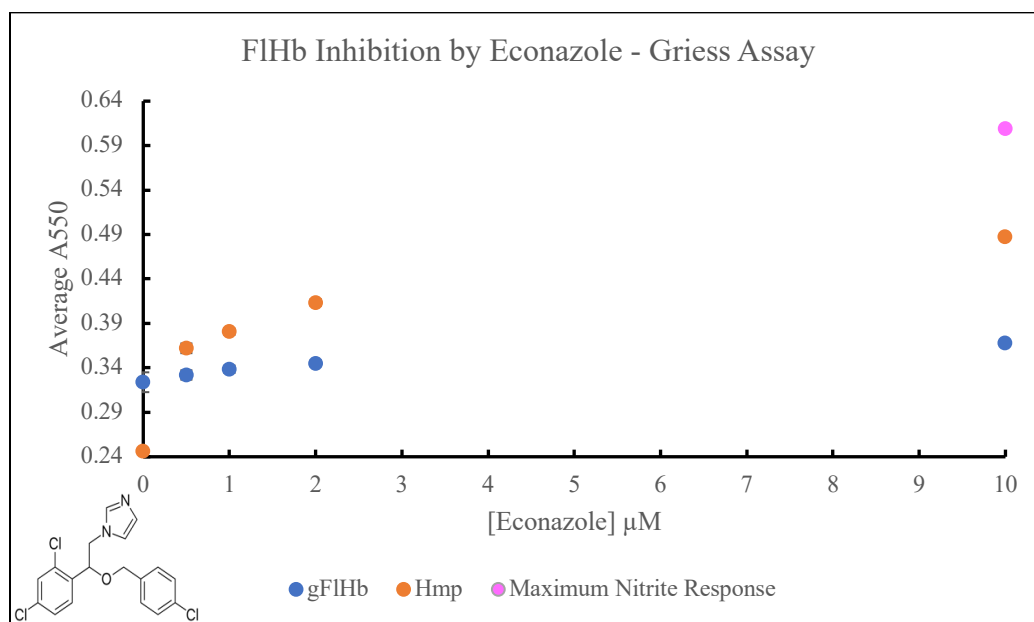
Figure 26: *Griess assay results assessing the NOD activity of FlHbs in the presence of econazole. Blue denotes the accumulation of nitrite in the experiments with gFlHb, and orange with Hmp. The pink circle indicates the maximum response for the full conversion of NO to nitrite by uncatalyzed oxidation with no flavohemoglobin present. This figure includes standard error bars, and each data point represents the mean value for n=6 wells.*

Figure 26 also shows how even though econazole appears to inhibit gFlHb to some

extent, it does not seem to be a very effective gFlHb inhibitor. These results align with those

obtained from the fluorescence assay (Figure 27), where it is more clear that Hmp is inhibited by

econazole at low concentrations (0.5 µM). This indicates that Hmp has a higher affinity for

econazole than gFlHb. These observations follow the same trend that was observed with

miconazole, where Hmp is inhibited to a greater degree at much lower concentrations than

gFlHb. The difference between the degree of inhibition for both enzymes becomes more evident

with the fluorescence assay (Figure 27), given its much more sensitive nature.
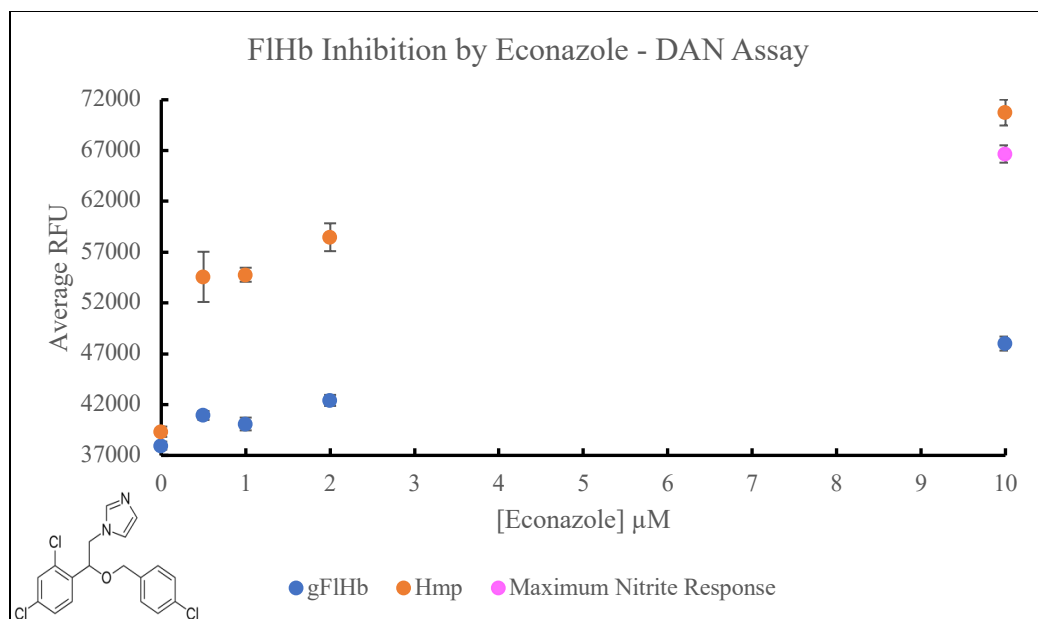
Figure 27: *Fluorescence assay results assessing the NOD activity of FlHbs in the presence of econazole. Blue denotes the accumulation of nitrite in the experiments with gFlHb, and orange with Hmp. The pink circle indicates the maximum response for the full conversion of NO to nitrite by uncatalyzed oxidation with no flavohemoglobin present. This figure includes standard error bars, and each data point represents the mean value for n=6 wells.*
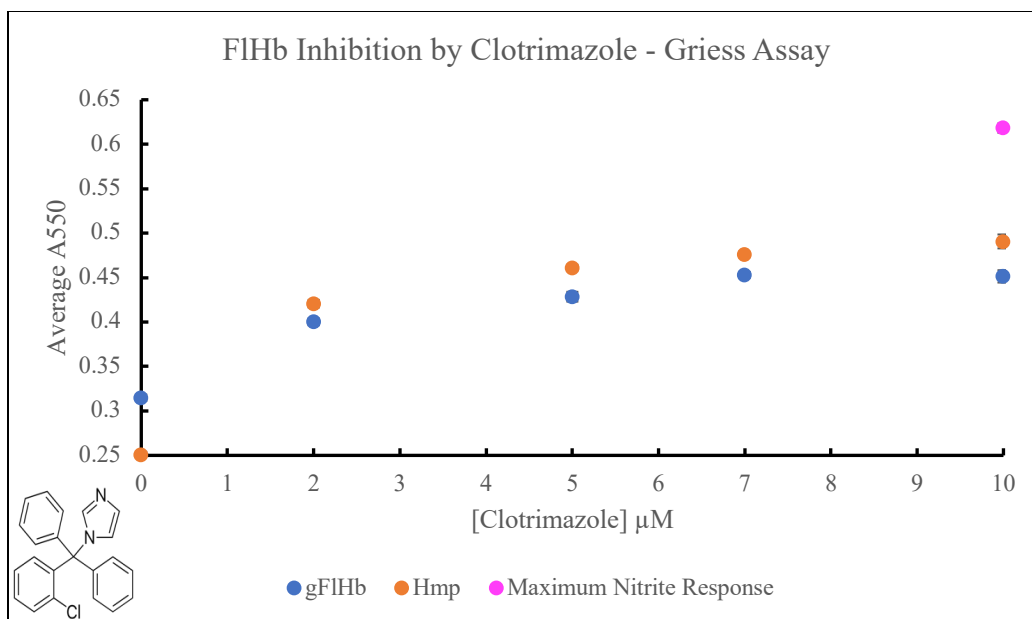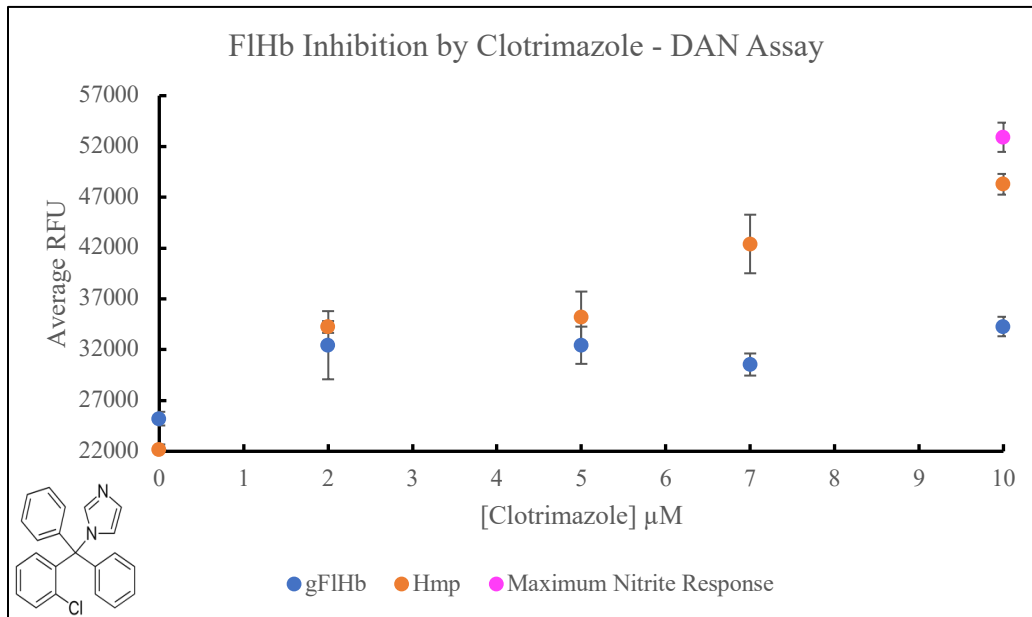
3.4.4 Clotrimazole

Clotrimazole is a bulkier compound than imidazole, but it is less bulky than miconazole, econazole, and ketoconazole. It has a molar mass of 344.84 g/mol and is the best gFlHb inhibitor, requiring relatively low concentrations (2-10 μM) to cause the partial inhibition of the enzyme. Its K_i for Hmp is 1,300 nM as determined by Helmick et al. (2005). The results from the Griess assay (Figure 28) and the fluorescence assay (Figure 29) exhibit the same trends. Both enzymes are only partially inhibited by clotrimazole, with Hmp having a higher affinity for the ligand as represented by higher absorbance and fluorescence measurements in both assays. The Griess assay (Figure 28) exhibits how the inhibition of both enzymes yields very similar nitrite concentrations upon the addition of the Griess reagents. The results obtained from the tests are very similar to one another, showing how clotrimazole partially inhibits both enzymes and indicating a similar affinity to the drug.

Figure 28: *Griess assay results assessing the NOD activity of FlHbs in the presence of clotrimazole. Blue denotes the accumulation of nitrite in the experiments with gFlHb, and orange with Hmp. The pink circle indicates the maximum response for the full conversion of NO to nitrite by uncatalyzed oxidation with no flavohemoglobin present. This figure includes standard error bars, and each data point represents the mean value for n=6 wells.*

Figure 29: *Fluorescence assay results assessing the NOD activity of FlHbs in the presence of clotrimazole. Blue denotes the accumulation of nitrite in the experiments with gFlHb, and orange with Hmp. The pink circle indicates the maximum response for the full conversion of NO to nitrite by uncatalyzed oxidation with no flavohemoglobin present. This figure includes standard error bars, and each data point represents the mean value for n=6 wells.*

The fluorescence assay (Figure 29) shows the same trend being followed, but the difference between the response from Hmp and gFlHb becomes more evident due to the much more sensitive nature of the fluorescence assay in comparison to the Griess Assay, thus suggesting that the affinity of Hmp for clotrimazole is higher than that of gFlHb to the same drug. It is also important to note that the concentrations of clotrimazole tested are much lower than those of imidazole, causing a similar response in gFlHb.

3.4.5 Ketoconazole

Ketoconazole was the largest compound that was tested in this study. It has a molar mass of 531.43 g/mol and a K_i of 5,000 nM for Hmp as reported by Helmick et al. (2005). The results from the Griess assay (Figure 30) and the fluorescence assay (Figure 31) exhibit how it partially inhibits both FlHbs.

Figure 30: *Griess assay results assessing the NOD activity of FlHbs in the presence of ketoconazole. Blue denotes the accumulation of nitrite in the experiments with gFlHb, and orange with Hmp. The pink circle indicates the maximum response for the full conversion of NO to nitrite by uncatalyzed oxidation with no flavohemoglobin present. This figure includes standard error bars, and each data point represents the mean value for n=6 wells.*
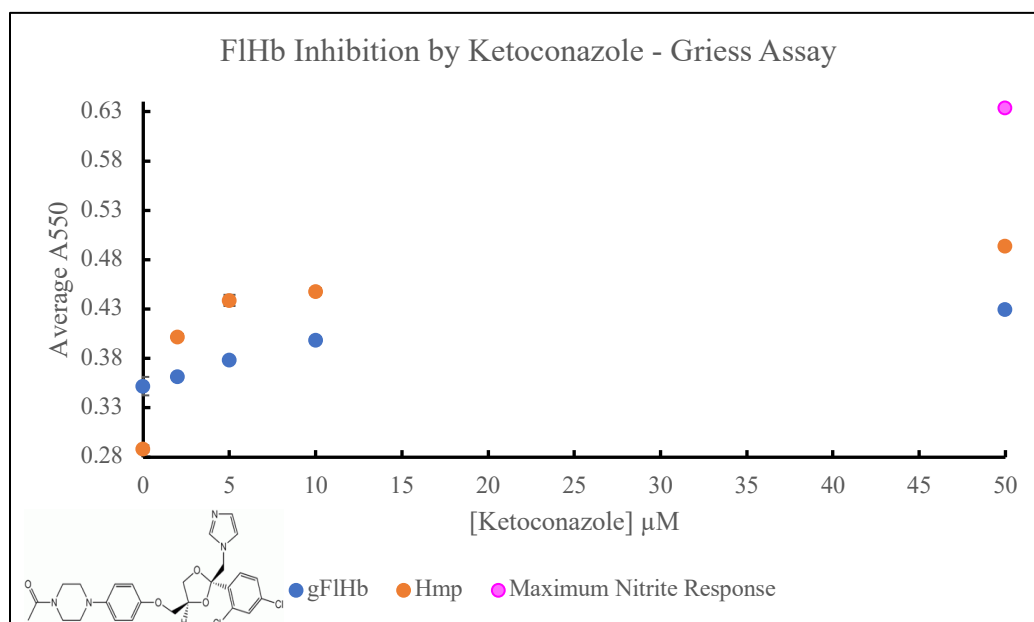
Once again, Hmp has a higher affinity for the drug, represented by higher NOD inhibition being observed. These results follow the same trend that is seen with miconazole, econazole, and clotrimazole, displaying how larger compounds are better at inhibiting the NOD activity of Hmp than that of gFlHb. The difference between the inhibition of Hmp and gFlHb becomes more evident with the fluorescence assay, due to the sensitive nature of this assay that allows for lower concentrations of nitrite to be effectively detected. This also follows the same trend that is observed with the other ligands. If well the Griess assay provides an accurate measurement of NOD inhibition, the fluorescence assay allows for the differences between these to become more obvious.
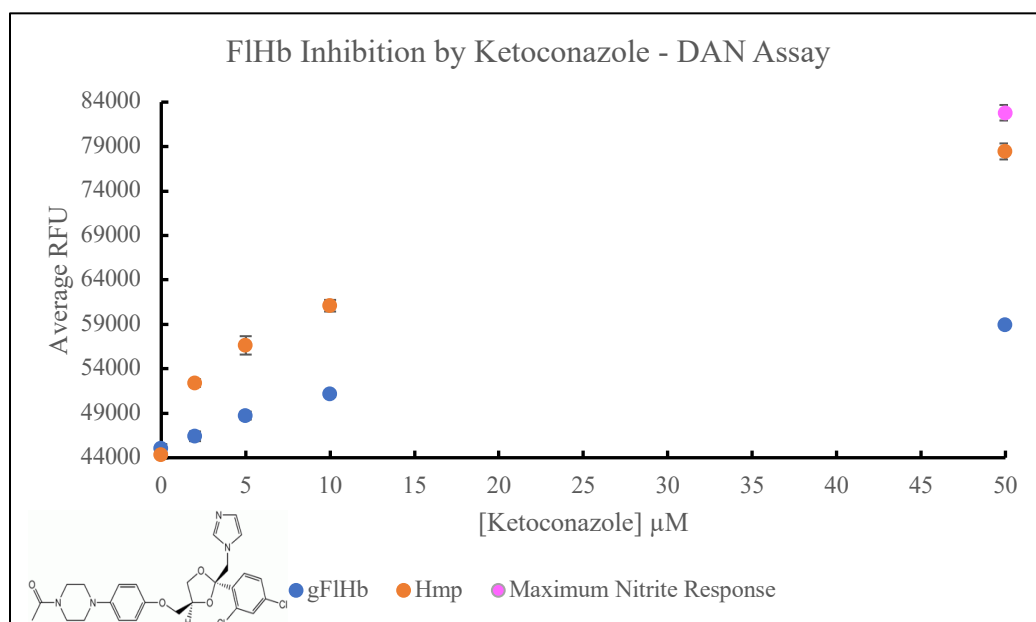
Figure 31: *Fluorescence assay results assessing the NOD activity of FlHbs in the presence of ketoconazole. Blue denotes the accumulation of nitrite in the experiments with gFlHb, and orange with Hmp. The pink circle indicates the maximum response for the full conversion of NO to nitrite by uncatalyzed oxidation with no flavohemoglobin present. This figure includes standard error bars, and each data point represents the mean value for n=6 wells.*

3.4.6 Metronidazole

Metronidazole is one of the two smallest compounds tested in this study, along with imidazole. It has a molar mass of 171.16 g/mol and is the preferred line of treatment for

giardiasis. It is because of this that it was tested to see if perhaps it had any effect in inhibiting the NOD activity of gFlHb and Hmp. The results of the Griess assay (Figure 32) and the fluorescence assay (Figure 33) are very straightforward and show no inhibition whatsoever being caused by metronidazole, represented by the lack of change in the absorbance and fluorescence measurements from the 0 µM metronidazole to the rest of the concentrations that were tested.

Figure 32: *Griess assay results assessing the NOD activity of FlHbs in the presence of metronidazole. Blue denotes the accumulation of nitrite in the experiments with gFlHb, and orange with Hmp. The pink circle indicates the maximum response for the full conversion of NO to nitrite by uncatalyzed oxidation with no flavohemoglobin present. This figure includes standard error bars, and each data point represents the mean value for n=3 wells.*

The lack of inhibition observed for both enzymes suggests that the Griess assay and the fluorescence assay are good tools for the screening of FlHb inhibitors as they effectively show when a ligand does simply not inhibit the enzymes as opposed to the intense responses seen with inhibition by other compounds. If metronidazole caused any inhibition of the FlHbs, it would be expected to cause a higher inhibition of gFlHb than Hmp as it is less bulky and would fit in the active site of the enzyme much easier than bulkier compounds like ketoconazole.
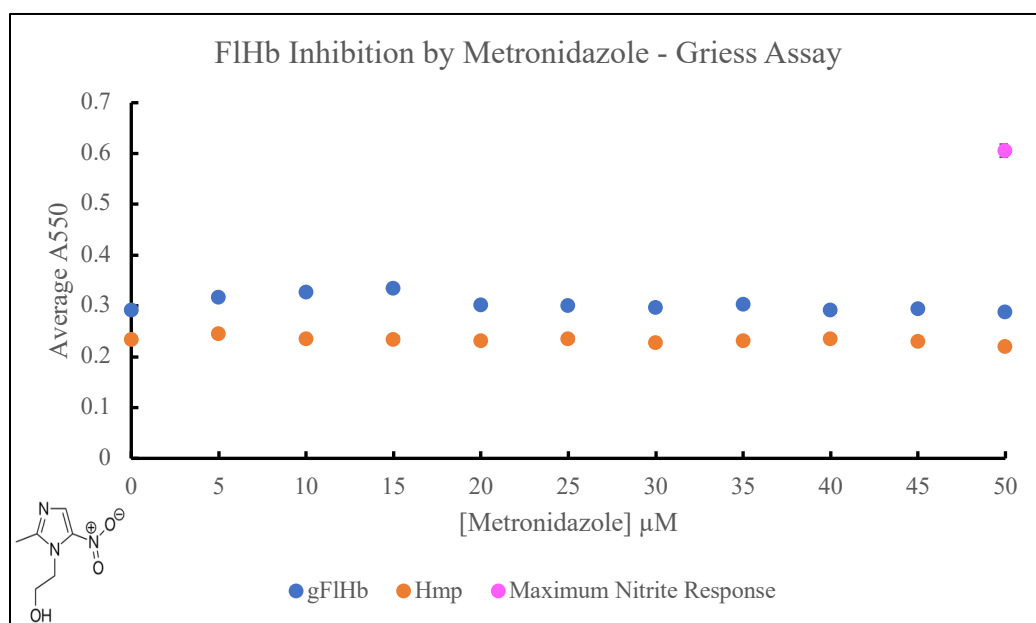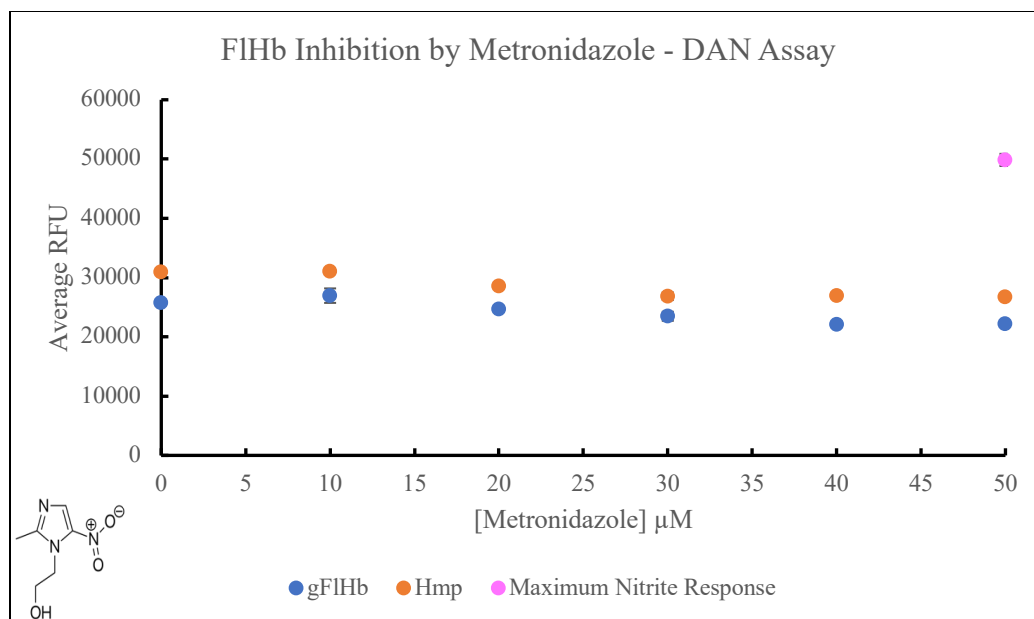
Figure 33: *Fluorescence assay results assessing the NOD activity of FlHbs in the presence of metronidazole. Blue denotes the accumulation of nitrite in the experiments with gFlHb, and orange with Hmp. The pink circle indicates the maximum response for the full conversion of NO to nitrite by uncatalyzed oxidation with no flavohemoglobin present. This figure includes standard error bars, and each data point represents the mean value for n=3 wells.*

Contrary to the other imidazole-based drugs that were selected for this study, based on previous studies pertaining to Hmp inhibition, metronidazole was selected due to genetic variations in gFlHb that are associated with metronidazole resistance (Saghaug et al., 2020). After exposure of Giardia to metronidazole gFlHb protein levels were increased, indicating that gFlHb may play a role in metronidazole tolerance. The study by Saghaug et al. (2020) reports how a variable number of gFlHb gene copies might be important for metronidazole tolerance by combating oxidative stress caused by the drug. Figure 32 and Figure 33 show how metronidazole does not elicit any NOD inhibitory response on Hmp or gFlHb, indicating that it is unlikely that the enzymes are binding to the drug. It is unlikely that metronidazole binds to FlHbs as the nitrogen on the drug that would coordinate to the heme iron is not able to do so because of a steric clash between the heme ring and the methyl group adjacent to the imidazole nitrogen of
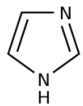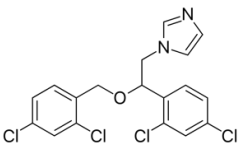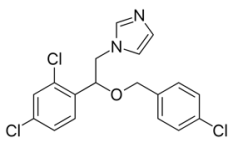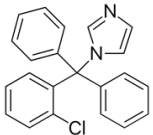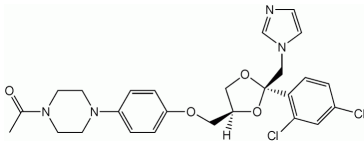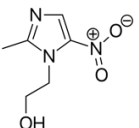
metronidazole. Therefore, it is unlikely that there is any direct association between metronidazole resistance and gFlHb.

3.4.7 General Remarks

Imidazole, miconazole, econazole, clotrimazole, and ketoconazole proved to inhibit gFlHb and Hmp to some extent (Table 5), as opposed to the case of metronidazole, where no inhibition was observed in these experiments (Figure 32 and Figure 33). While most of these compounds only caused the partial inhibition of both FlHbs, two compounds stood out from the rest. Imidazole was the only inhibitor from the tested compounds that better inhibited the NOD activity of gFlHb than that of Hmp (Figure 22 and Figure 23). The other compound that stood out was miconazole as it was the only compound that came close to causing the complete inhibition of the NOD activity of Hmp as seen in Figure 24 and Figure 25. Nonetheless, miconazole's inhibition was expected based on the K_i values found in the literature.

Other than the case of imidazole, the NOD activity of Hmp was more affected than that of gFlHb by the different inhibitors (Table 5). The unique pair of sequence inserts found in the globin domain and the FNR domain of gFlHb are predicted to increase the interdomain contact surface of gFlHb compared to other FlHbs. These interactions are predicted to interfere with substrate entry, affecting the binding of larger compounds to gFlHb's active site. By increasing the interdomain contact surface, these inserts decrease the surface area of the heme pocket, thus restricting the access of larger compounds to the active site. These predictions align with the results of this study as larger imidazole-based compounds inhibited Hmp better than they inhibited gFlHb (Table 5).

Table 5: *FlHb Sensitivity to Tested Ligands*

Ligand	Structure	Which FlHb is More Sensitive?
Imidazole		gFlHb
Miconazole		Hmp
Econazole		Hmp
Clotrimazole		Hmp
Ketoconazole		Hmp
Metronidazole		No Inhibition

3.5 Future Directions

It is thought that gFlHb plays a vital role in Giardia to combat the stress that arises from RNS and ROS produced by the host's immune response. It is because of this that gFlHb could be a potential target for the treatment of giardiasis and that screening for effective gFlHb inhibitors could ultimately lead to the development of anti-giardia drugs. Nonetheless, this is all based on studies that assess the NOD activity of gFlHb as an isolated protein. To date, there have not been any knockout studies where the gFlHb sequence is deleted from the organism. *In vivo* studies

that deal with the deletion of the gFlHb gene would be required to evaluate whether this enzyme plays a vital role in RNS and ROS detoxification by evaluating the effects of these reactive species on giardia as a whole, in the absence of gFlHb.

Upon the adaptation, development, and optimization of the Griess and fluorescence assays, only six compounds were tested due to time limitations and a lack of previous research on imidazole-based drugs and Hmp. These assays, now working assays, can be used to screen a potential library of compounds with similar characteristics to the ones that were already tested based on predicted interactions of these ligands with gFlHb based on homology models constructed from Hmp. Crystallographic studies would also be required to obtain an accurate model of gFlHb as, to date, all existing models are based on the homology of gFlHb and Hmp.

The Griess and fluorescence assays have the potential to be used in the screening of FlHb inhibitors not only in giardia but in other organisms such as yeast. The scope of the assays could be expanded to screen for FlHb inhibitors and analyze how their responses differ based on the structural differences of these enzymes. This could ultimately lead to a better understanding of this group of enzymes and their behavior.

3.6 Conclusions

The NOD activity of Hmp is much more efficient than that of gFlHb as evidenced by Figures 22-33. The absorbance and fluorescent measurements of the uninhibited NOD reaction tend to yield lower nitrite concentrations in Hmp than gFlHb. This indicates that Hmp has a more efficient NOD activity that allows for the successful conversion of NO to nitrate.

The Griess and fluorescence assays are efficient tools to screen for FlHb inhibitors as they are successfully able to detect nitrite concentrations in a solution as a result of the inhibition of the NOD activity. These assays also exhibit isotype selectivity, supported by different

responses of each enzyme to different ligands. Different ligands elicit different responses in gFlHb and Hmp, the Griess and fluorescence assays are able to detect these differences and provide different results for both enzymes that can then be compared to one another in order to determine whether an enzyme is more susceptible to a specific ligand. These differences play a vital role in screening for gFlHb inhibitors as, ideally, a good gFlHb inhibitor would successfully inhibit the enzyme while causing a mild response from Hmp, which is present in the commensal gut bacteria *E. coli*.

The Griess and fluorescence assays offer a rapid, simple, non-expensive high-throughput method to screen for FlHb inhibitors. The existing drug screening tools are usually expensive and time-consuming. These assays offer a quick and cheap alternative to screen for various compounds in the span of hours.

4. REFERENCES

Adam, R. D. (2001). Biology of Giardia lamblia. *Clinical Microbiology Reviews*, *14*(3), 447–475. https://doi.org/10.1128/CMR.14.3.447-475.2001

Bonamore, A., & Boffi, A. (2008). Flavohemoglobin: Structure and reactivity. *IUBMB Life*, *60*(1), 19–28. https://doi.org/10.1002/iub.9

Brown, D. M., Upcroft, J. A., & Upcroft, P. (1995). Free radical detoxification in Giardia duodenalis. *Molecular and Biochemical Parasitology*, *72*, 47–56. https://doi.org/https://doi.org/10.1016/0166-6851(95)00065-9

Brown, D. M., Upcroft, J. A., & Upcroft, P. (1996). A H2O-producing NADH oxidase from the protozoan parasite Giardia duodenalis. *European Journal of Biochemistry*, *241*(1), 155–161. https://doi.org/10.1111/j.1432-1033.1996.0155t.x

Bryan, N. S., & Grisham, M. B. (2007). Methods to Detect Nitric Oxide and its Metabolites in Biological Samples. *Free Radical Biology and Medicine*, *43*(5), 645–657. https://doi.org/https://doi.org/10.1016%2Fj.freeradbiomed.2007.04.026

Cama, V. A., & Mathison, B. A. (2015). Infections by Intestinal Coccidia and Giardia duodenalis. In *Clinics in Laboratory Medicine* (Vol. 35, Issue 2, pp. 423–444). W.B. Saunders. https://doi.org/10.1016/j.cll.2015.02.010

Damiani, P., & Burini, G. (1986). Fluorometric Determination of Nitrite. *Talanta*, *33*(8), 649–652. https://doi.org/https://doi.org/10.1016/0039-9140(86)80151-5

Di Matteo, A., Scandurra, F. M., Testa, F., Forte, E., Sarti, P., Brunori, M., & Giuffrè, A. (2008). The O2-scavenging flavodiiron protein in the human parasite Giardia intestinalis. *Journal of Biological Chemistry*, *283*(7), 4061–4068. https://doi.org/10.1074/jbc.M705605200

Ellis, J. E., Williams, R., Cole, D., Cammack, R., & Lloyd, D. (1993). Electron transport components of the parasitic protozoon Giardia lamblia. *FEBS Letters*, *325*(3), 196–200. https://doi.org/10.1016/0014-5793(93)81072-8

Ermler, U., Siddiqui, R. A., Cramm, R., & Friedrich, B. (1995). Crystal structure of the flavohemoglobin from alcaligenes eutrophus at 1.75 Å resolution. *EMBO Journal*, *14*(24), 6067–6077. https://doi.org/10.1002/j.1460-2075.1995.tb00297.x

Fantinatti, M., Bello, A. R., Fernandes, O., & Da-Cruz, A. M. (2016). Identification of Giardia lamblia Assemblage e in Humans Points to a New Anthropozoonotic Cycle. *Journal of Infectious Diseases*, *214*(8), 1256–1259. https://doi.org/10.1093/infdis/jiw361

Farthing, M. J. G. (1993). Diarrhoeal disease: current concepts and future challenges Pathogenesis of giardiasis. *Transactions of the Royal Society of Tropical Medicine and Hygiene*, *87*(Supplement 3), 17–21. https://doi.org/https://doi.org/10.1016/0035-9203(93)90531-t

Gardner, P. R., Gardner, A. M., Martin, L. A., & Salzman, A. L. (1998). Nitric oxide dioxygenase: An enzymic function for flavohemoglobin. *PNAS*, *95*, 10378–10383. https://doi.org/https://doi.org/10.1073/pnas.95.18.10378

Griess, J. P. (1879). Bemerkungen zu der Abhandlung der HH. Weselsky und Benedikt „Ueber einige Azoverbindungen. *Ber. Dtsch. Chem. Ges.*, *12*, 426–428. https://doi.org/https://doi.org/10.1002/cber.187901201117

Grisham, M. B., Johnson, G. G., & Lancaster, J. R. (1996). Nitrate and Nitrite in Extracellular Fluids. *Methods in Enzymology*, *268*, 237–246. https://doi.org/https://doi.org/10.1016/s0076-6879(96)68026-4

Helmick, R. A., Fletcher, A. E., Gardner, A. M., Gessner, C. R., Hvitved, A. N., Gustin, M. C., & Gardner, P. R. (2005). Imidazole antibiotics inhibit the nitric oxide dioxygenase function of microbial flavohemoglobin. *Antimicrobial Agents and Chemotherapy*, *49*(5), 1837–1843. https://doi.org/10.1128/AAC.49.5.1837-1843.2005

Ignarro, L. J., Fukuto, J. M., Griscavage, J. M., Rogers, N. E., & Byrns, R. E. (1993). Oxidation of nitric oxide in aqueous solution to nitrite but not nitrate: Comparison with enzymatically formed nitric oxide from L-arginine. *PNAS*, *90*, 8103–8107. https://doi.org/https://doi.org/10.1073/pnas.90.17.8103

Ilari, A., & Boffi, A. (2008). Structural Studies on Flavohemoglobins. In *Methods in Enzymology* (Vol. 436, pp. 187–202). Academic Press Inc. https://doi.org/10.1016/S0076-6879(08)36010-8

Ilari, A., Bonamore, A., Farina, A., Johnson, K. A., & Boffi, A. (2002). The X-ray structure of ferric Escherichia coli flavohemoglobin reveals an unexpected geometry of the distal heme pocket. *Journal of Biological Chemistry*, *277*(26), 23725–23732. https://doi.org/10.1074/jbc.M202228200

Jumper, J., Evans, R., Pritzel, A., Green, T., Figurnov, M., Ronneberger, O., Tunyasuvunakool, K., Bates, R., Žídek, A., Potapenko, A., Bridgland, A., Meyer, C., Kohl, S. A. A., Ballard, A. J., Cowie, A., Romera-Paredes, B., Nikolov, S., Jain, R., Adler, J., … Hassabis, D. (2021). Highly accurate protein structure prediction with AlphaFold. *Nature*, *596*(7873), 583–589. https://doi.org/10.1038/s41586-021-03819-2

Lane, S., & Lloyd, D. (2002). Current trends in research into the waterborne parasite Giardia. In *Critical Reviews in Microbiology* (Vol. 28, Issue 2, pp. 123–147). CRC Press LLC. https://doi.org/10.1080/1040-840291046713

Leitsch, D., Williams, C. F., & Hrdý, I. (2018). Redox Pathways as Drug Targets in Microaerophilic Parasites. *Trends in Parasitology*, *34*(7), 576–589. https://doi.org/10.1016/j.pt.2018.04.007

Leung, A. K. C., Leung, A. A. M., Wong, A. H. C., Sergi, C. M., & Kam, J. K. M. (2019). Giardiasis: an overview. *Recent Patents on Inflammation & Allergy Drug Discovery*, *13*(2). https://doi.org/10.2174/1872213x13666190618124901

Li, L., & Wang, C. C. (2006). A likely molecular basis of the susceptibility of Giardia lamblia towards oxygen. *Molecular Microbiology*, *59*(1), 202–211. https://doi.org/10.1111/j.1365-2958.2005.04896.x

Lin, M., Wang, Z., Fang, H., Liu, L., Yin, H., Yan, C. H., & Fu, X. (2016). Metal-free aerobic oxidative coupling of amines in dimethyl sulfoxide via a radical pathway. *RSC Advances*, *6*(13), 10861–10864. https://doi.org/10.1039/c5ra25434e

Lloyd, D., Harris, J. C., Maroulis, S., Biagini, G. A., Wadley, R. B., Turner, M. P., & Edwards, M. R. (2000). The microaerophilic flagellate Giardia intestinalis: oxygen and its reaction products collapse membrane potential and cause cytotoxicity. In *Microbiology* (Vol. 146). https://doi.org/https://doi.org/10.1099/00221287-146-12-3109

Markarian, S. A., & Shahinyan, G. A. (2015). The effect of dimethylsulfoxide on absorption and fluorescence spectra of aqueous solutions of acridine orange base. *Spectrochimica Acta - Part A: Molecular and Biomolecular Spectroscopy*, *151*, 662–666. https://doi.org/10.1016/j.saa.2015.06.126

Marshall, M. M., Naumovitz, D., Ortega, Y., & Sterling, C. R. (1997). Waterborne Protozoan Pathogens. *Clinical Microbiology Reviews*, *10*(1), 67–85. https://doi.org/https://doi.org/10.1128/cmr.10.1.67

Mastronicola, D., Falabella, M., Forte, E., Testa, F., Sarti, P., & Giuffrè, A. (2016). Antioxidant defence systems in the protozoan pathogen Giardia intestinalis. *Molecular and Biochemical Parasitology*, *206*(1–2), 56–66. https://doi.org/10.1016/j.molbiopara.2015.12.002

Mastronicola, D., Falabella, M., Testa, F., Pucillo, L. P., Teixeira, M., Sarti, P., Saraiva, L. M., & Giuffrè, A. (2014). Functional Characterization of Peroxiredoxins from the Human Protozoan Parasite Giardia intestinalis. *PLoS Neglected Tropical Diseases*, *8*(1), 35. https://doi.org/10.1371/journal.pntd.0002631

Mastronicola, D., Testa, F., Forte, E., Bordi, E., Pucillo, L. P., Sarti, P., & Giuffrè, A. (2010). Flavohemoglobin and nitric oxide detoxification in the human protozoan parasite Giardia intestinalis. *Biochemical and Biophysical Research Communications*, *399*(4), 654–658. https://doi.org/10.1016/j.bbrc.2010.07.137

Misko, T. P., Schilling, R. J., Salvemini, D., Moore, W. M., & Currie, M. G. (1993). A Fluorometric Assay for the Measurement of Nitrite in Biological Samples. *Analytical Biochemistry*, *214*, 11–16. https://doi.org/https://doi.org/10.1006/abio.1993.1449

Moody, J. A., & Shaw, F. L. (2006). Reevaluation of the Griess reaction: How much of a problem is interference by nicotinamide nucleotides? *Analytical Biochemistry*, *356*(1), 154–156. https://doi.org/10.1016/j.ab.2006.05.026

Mørch, K., & Hanevik, K. (2020). Giardiasis treatment: an update with a focus on refractory disease. In *Current Opinion in Infectious Diseases* (Vol. 33, Issue 5, pp. 355–364). Lippincott Williams and Wilkins. https://doi.org/10.1097/QCO.0000000000000668

Mukai, M., Mills, C. E., Poole, R. K., & Yeh, S. R. (2001). Flavohemoglobin, a Globin with a Peroxidase-like Catalytic Site. *Journal of Biological Chemistry*, *276*(10), 7272–7277. https://doi.org/10.1074/jbc.M009280200

Nam, J., Jung, I. B., Kim, B., Lee, S. M., Kim, S. E., Lee, K. N., & Shin, D. S. (2018). A colorimetric hydrogel biosensor for rapid detection of nitrite ions. *Sensors and Actuators, B: Chemical*, *270*, 112–118. https://doi.org/10.1016/j.snb.2018.04.171

Nezamololama, N. (2019). *Ligand Binding Properties of Giardia Flavohemoglobin* [M.Sc. Thesis].

Ollesch, G., Kaunzinger, A., Juchelka, D., Schubert-Zsilavecz, M., & Ermler, U. (1999). Phospholipid bound to the flavohemoprotein from Alcaligenes eutrophus. *European Journal of Biochemistry*, *262*(2), 396–405. https://doi.org/10.1046/j.1432-1327.1999.00381.x

Olson, M. E., Ceri, H., & Morck, D. W. (2000). Giardia Vaccination. *Parasitology Today*, *16*(5), 213–217. https://doi.org/https://doi.org/10.1016/S0169-4758(99)01623-3

Ortega, Y. R., & Adam, R. D. (1997). Giardia: Overview and Update. *Clinical Infectious Diseases*, *25*(3), 545–550. https://doi.org/https://doi.org/10.1086/513745

Ozcan, A., & Ogun, M. (2015). Biochemistry of Reactive Oxygen and Nitrogen Species. In *Basic Principles and Clinical Significance of Oxidative Stress*. InTech. https://doi.org/10.5772/61193

Phaniendra, A., Jestadi, D. B., & Periyasamy, L. (2015). Free Radicals: Properties, Sources, Targets, and Their Implication in Various Diseases. In *Indian Journal of Clinical Biochemistry* (Vol. 30, Issue 1, pp. 11–26). Springer India. https://doi.org/10.1007/s12291-014-0446-0

Poole, R. K. (2020). Flavohaemoglobin: The pre-eminent nitric oxide-detoxifying machine of microorganisms. *F1000Research*, *9*. https://doi.org/10.12688/f1000research.20563.1

Rafferty, S., Luu, B., March, R. E., & Yee, J. (2010). Giardia lamblia encodes a functional flavohemoglobin. *Biochemical and Biophysical Research Communications*, *399*(3), 347–351. https://doi.org/10.1016/j.bbrc.2010.07.073

Rafferty, S. P., & Dayer, G. (2015). Heme proteins of Giardia intestinalis. In *Experimental Parasitology* (Vol. 159, pp. 13–23). Academic Press Inc. https://doi.org/10.1016/j.exppara.2015.08.001

Rehder, D. (2014). *Bioinorganic Chemistry*. Oxford University Press.

Saghaug, C. S., Klotz, C., Kallio, J. P., Aebischer, T., Langeland, N., & Hanevik, K. (2020). Genetic diversity of the flavohemoprotein gene of giardia lamblia: Evidence for high allelic heterozygosity and copy number variation. *Infection and Drug Resistance*, *13*, 4531–4545. https://doi.org/10.2147/IDR.S274543

Savioli, L., Smith, H., & Thompson, A. (2006). Giardia and Cryptosporidium join the "Neglected Diseases Initiative." *Trends in Parasitology*, *22*(5), 203–208. https://doi.org/10.1016/j.pt.2006.02.015

Sun, J., Zhang, X., Broderick, M., & Fein, H. (2003). Measurement of Nitric Oxide Production in Biological Systems by Using Griess Reaction Assay. *Sensors*, *3*, 276–284. https://doi.org/https://doi.org/10.3390/s30800276

Testa, F., Mastronicola, D., Cabelli, D. E., Bordi, E., Pucillo, L. P., Sarti, P., Saraiva, L. M., Giuffrè, A., & Teixeira, M. (2011). The superoxide reductase from the early diverging eukaryote Giardia intestinalis. *Free Radical Biology and Medicine*, *51*(8), 1567–1574. https://doi.org/10.1016/j.freeradbiomed.2011.07.017

Tovar, J., León-Avila, G., Sánchez, L. B., Sutak, R., Tachezy, J., van der Giezen, M., Hernández, M., Müller, M., & Lucocq, J. M. (2003). Mitochondrial remnant organelles of Giardia function in iron-sulphur protein maturation. *Nature*, *426*(6963), 172–176. https://doi.org/https://doi.org/10.1038/nature01945

Tsikas, D. (2007). Analysis of nitrite and nitrate in biological fluids by assays based on the Griess reaction: Appraisal of the Griess reaction in the l-arginine/nitric oxide area of research. In *Journal of Chromatography B: Analytical Technologies in the Biomedical and Life Sciences* (Vol. 851, Issues 1–2, pp. 51–70). https://doi.org/10.1016/j.jchromb.2006.07.054

Vanden Bossche, H., Engelen, M., & Rochette, F. (2003). Antifungal agents of use in animal health - Chemical, biochemical and pharmacological aspects. *Journal of Veterinary Pharmacology and Therapeutics*, *26*(1), 5–29. https://doi.org/10.1046/j.1365-2885.2003.00456.x